Article

Cell Metabolism

The TORC1-Regulated CPA Complex Rewires an RNA Processing Network to Drive Autophagy and Metabolic Reprogramming

Graphical Abstract

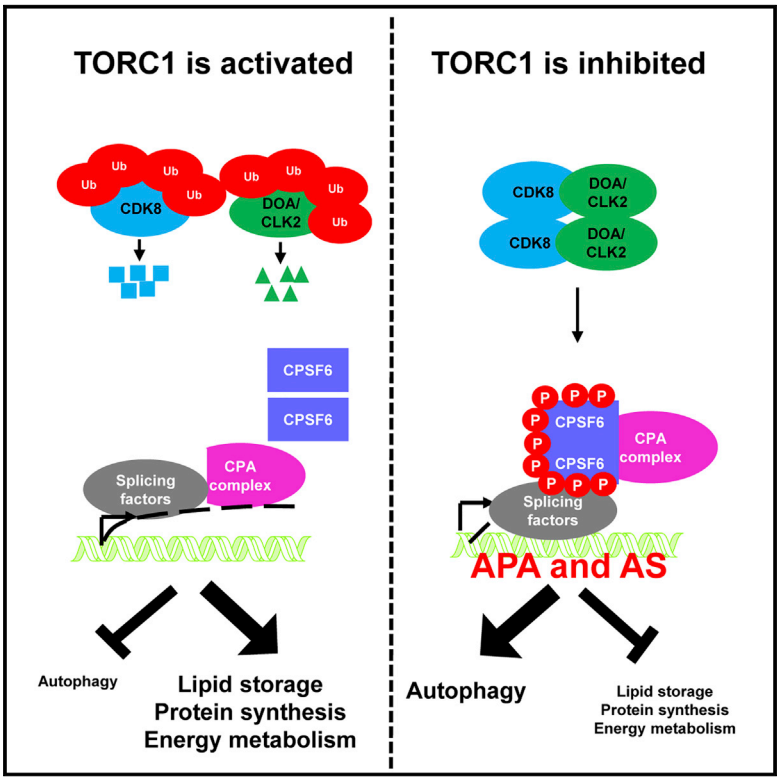

Highlights

- TORC1 negatively inhibits CDK8 and DOA kinases
- CDK8 and DOA phosphorylate CPSF6 to induce alternative RNA processing
- Depletion of CPSF6 impairs autophagy and metabolic changes during starvation
- The CDK8-CLK2/DOA-CPSF6 axis is conserved in mammals

Authors

Hong-Wen Tang, Yanhui Hu, Chiao-Lin Chen, ..., John M. Asara, Leonard Rabinow, Norbert Perrimon

Correspondence

hwtang@genetics.med.harvard.edu (H.-W.T.), perrimon@receptor.med.harvard.edu (N.P.)

In Brief

Tang et al. investigate the mechanisms of how TORC1 regulates autophagy and cell metabolism. They demonstrate that CDK8 and DOA, two kinases downstream of TORC1 signaling, directly phosphorylate CPSF6 to regulate alternative mRNA polyadenylation and splicing and mediate TORC1-dependent physiological functions.

Tang et al., 2018, Cell Metabolism *27*, 1–15
May 1, 2018
https://doi.org/10.1016/j.cmet.2018.02.023

CellPress

Please cite this article in press as: Tang et al., The TORC1-Regulated CPA Complex Rewires an RNA Processing Network to Drive Autophagy and Metabolic Reprogramming, Cell Metabolism (2018), https://doi.org/10.1016/j.cmet.2018.02.023

The TORC1-Regulated CPA Complex Rewires an RNA Processing Network to Drive Autophagy and Metabolic Reprogramming

Hong-Wen Tang,[1,*] Yanhui Hu,[1] Chiao-Lin Chen,[1] Baolong Xia,[1] Jonathan Zirin,[1] Min Yuan,[3,4] John M. Asara,[3,4] Leonard Rabinow,[1] and Norbert Perrimon[1,2,5,*]
[1]Department of Genetics, Harvard Medical School, 77 Avenue Louis Pasteur, Boston, MA 02115, USA
[2]Howard Hughes Medical Institute, 77 Avenue Louis Pasteur, Boston, MA 02115, USA
[3]Department of Medicine, Harvard Medical School, Boston, MA 02115, USA
[4]Division of Signal Transduction, Beth Israel Deaconess Medical Center, Boston, MA 02115, USA
[5]Lead Contact
*Correspondence: hwtang@genetics.med.harvard.edu (H.-W.T.), perrimon@receptor.med.harvard.edu (N.P.)
https://doi.org/10.1016/j.cmet.2018.02.023

SUMMARY

Nutrient deprivation induces autophagy through inhibiting TORC1 activity. We describe a novel mechanism in *Drosophila* by which TORC1 regulates RNA processing of *Atg* transcripts and alters ATG protein levels and activities via the cleavage and polyadenylation (CPA) complex. We show that TORC1 signaling inhibits CDK8 and DOA kinases, which directly phosphorylate CPSF6, a component of the CPA complex. These phosphorylation events regulate CPSF6 localization, RNA binding, and starvation-induced alternative RNA processing of transcripts involved in autophagy, nutrient, and energy metabolism, thereby controlling autophagosome formation and metabolism. Similarly, we find that mammalian CDK8 and CLK2, a DOA ortholog, phosphorylate CPSF6 to regulate autophagy and metabolic changes upon starvation, revealing an evolutionarily conserved mechanism linking TORC1 signaling with RNA processing, autophagy, and metabolism.

INTRODUCTION

Autophagy is a conserved process by which cells recycle macromolecules or organelles engulfed by specialized double-membraned vesicles called autophagosomes. Autophagosomes fuse with lysosomes, where their inner membranes and contents are degraded by hydrolases. This degradative process can provide energy or resources to maintain homeostasis during various environmental stresses, and is implicated in many biological processes and diseases (Jiang and Mizushima, 2014). More than 30 autophagy-related (ATG) genes were identified in yeast, and most of them are conserved in mammals. These ATG proteins can be classified into six functional units and, among them, the ATG1 kinase complex (ATG1/ATG13/FIP200) is the central autophagic regulator (Ohsumi, 2014). ATG1 interacts with ATG13 and FIP200 to serve as a scaffold for recruitment of other ATG proteins to the pre-autophagosomal structure, initiating autophagy (Cheong et al., 2008). ATG1 also regulates other functional units to control different stages of autophagosome formation (Mercer et al., 2018). In *Drosophila*, *Atg1* overexpression is sufficient to induce autophagy, highlighting its critical role (Scott et al., 2007).

Various signaling pathways regulate autophagy. For example, cAMP-dependent protein kinase A (PKA) directly phosphorylates Atg1 and Atg13 to inhibit autophagy in yeast and mammals (Budovskaya et al., 2005; Dorsey et al., 2009; Stephan et al., 2009). AMP-activated protein kinase directly phosphorylates ULK1 (the mammalian ortholog of Atg1) and Beclin 1 to activate autophagy in mammals (Mihaylova and Shaw, 2011). Moreover, the phosphatidylinositol 3-kinase (PI3K)/AKT/TORC1 pathway links hormonal signaling and nutritional status to autophagy in response to starvation, as TORC1 blocks autophagy through direct phosphorylation of ULK1 (Kim et al., 2011). Interestingly, a recent study reported that mammalian target of rapamycin mediates the phosphorylation of an mRNA de-capping complex, RCK/Dcp2, to degrade *Atg* transcripts, suppressing autophagy (Hu et al., 2015). Thus, TORC1 regulates autophagy at multiple steps.

From a genetic screen in *Drosophila*, we identified the cleavage and polyadenylation (CPA) complex as a novel regulator of autophagy. The CPA complex consists of more than 20 proteins classified into four sub-complexes and several single proteins and is required for cleavage and polyadenylation of pre-mRNAs. The sub-complexes include the evolutionarily conserved cleavage and polyadenylation specificity factor (CPSF), cleavage stimulation factor (CstF), cleavage factor I (CFI), and CFII subcomplexes (Chan et al., 2011; Table S1). Here, we characterize the role of the CPA complex in autophagy and demonstrate that it coordinates alternative polyadenylation ([APA], a mechanism that generates distinct 3′ UTRs on mRNAs) of *Atg1* and *Atg8a* transcripts, with alternative splicing (AS, a mechanism that joins different exons to form mRNAs isoforms) of *Atg1*. CPA activity increases ATG protein levels and ATG1 kinase complex formation, enhancing autophagy during nutrient starvation. Importantly, these RNA processing events are regulated by TORC1 signaling. We show that TORC1 activity negatively regulates two downstream kinases, CDK8 and DOA, which directly

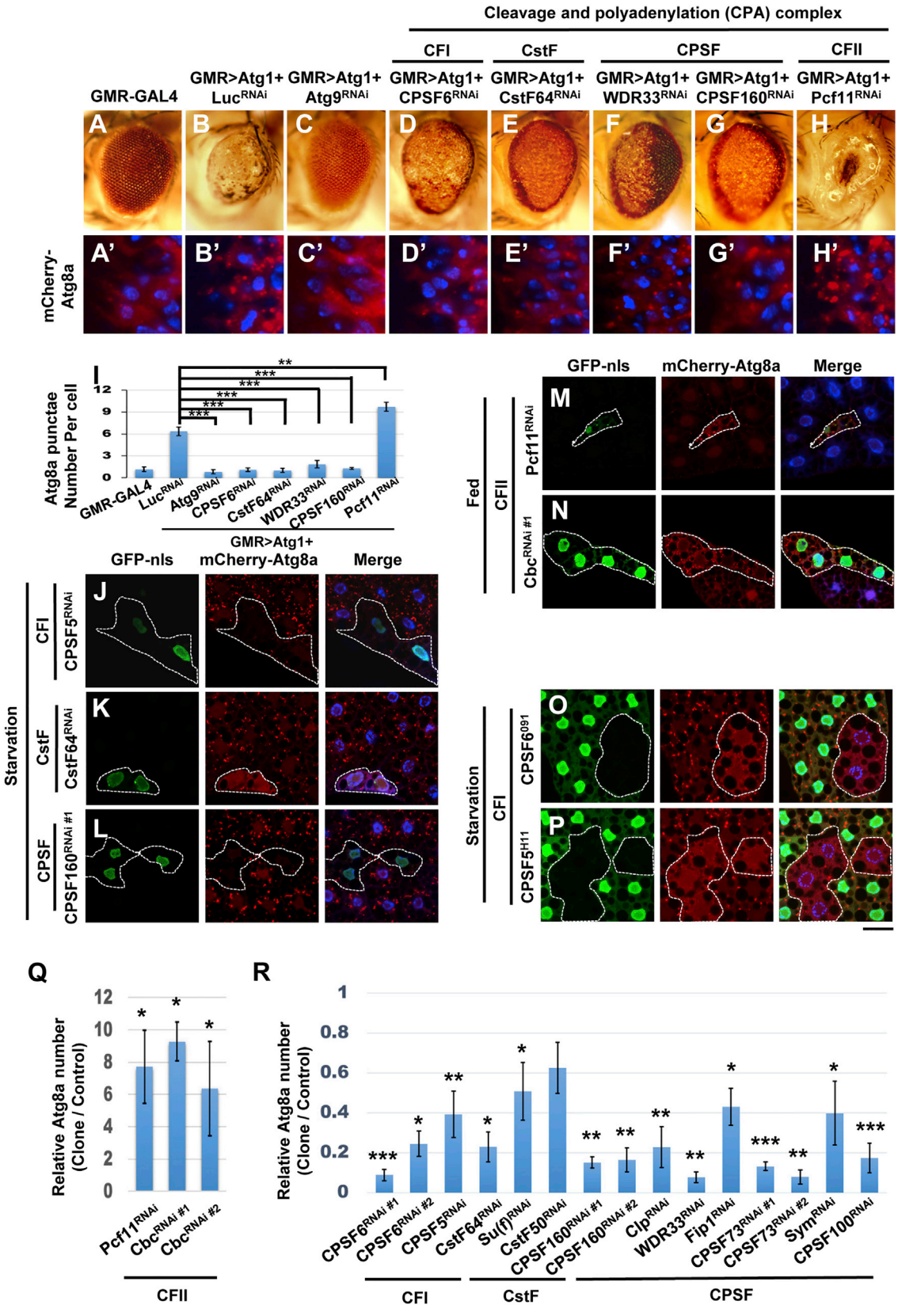

(legend on next page)

phosphorylate CPSF6 (CG7185), a key component of the CPA complex, controlling its nuclear localization and RNA-binding ability. Significantly, depletion of *CDK8*, *DOA*, or *CPSF6*, compromises starvation-induced autophagy and also causes energy, lipid, and protein metabolic defects in both *Drosophila* and mammalian cells. Our studies thus identify a new role for the CPA complex in mediating TORC1-dependent functions and demonstrate that TORC1 controls alternative RNA processing through CDK8/DOA/CPA signaling.

RESULTS

Modifiers of *Atg1*-Mediated Autophagy

Overexpression of *Atg1* in the *Drosophila* eye induces autophagy, leading to reduced eye size and a rough eye phenotype (Figures 1A and 1B) (Chen et al., 2008; Scott et al., 2007). To identify new autophagic regulators, we overexpressed ATG1 in the eye and performed an RNAi screen for modifiers. The *Atg1*-induced eye phenotype is rescued by *Atg9-RNAi*, suggesting that these phenotypes are autophagy dependent (Figure 1C). While depletion of *PCF11* (a CFII sub-complex component) enhanced the *Atg1*-induced rough eye phenotype, multiple RNAi lines against other sub-complex components of the CPA complex, including CPSF6 (CFI complex), CstF64 (CstF complex), WDR33, and CPSF160 (CPSF complex), rescued the rough eye phenotype (Figures 1D–1H). Furthermore, co-expression of the autophagosomal marker mCherry-ATG8a with *Atg1* induced mcherryATG8a punctae formation in third-instar larval eye discs (compare Figures 1A′, 1B′, and 1I). These ATG8a punctae were abolished by depletion of *Atg9*, *CPSF6*, *CstF64*, *WDR33*, or *CPSF160*, while *PCF11-RNAi* increased their prevalence (Figures 1 C′–1H′ and 1I). Thus, the CFI, CPSF, and CstF sub-complexes are required for *Atg1*-induced autophagosome formation, and the CFII sub-complex has the opposite function.

We next examined the effects of CPA complex components on starvation-induced autophagy in the larval fat body. Consistently, depletion of CFI, CPSF, or the CstF sub-complex suppressed starvation-induced mCherryATG8a punctae formation, whereas reducing CFII sub-complex expression increased ATG8a punctae under fed conditions (Figures 1J–1N and 1Q–1R). To further confirm this result, we generated null mutations in components of the CFI sub-complex, *CPSF5* and *CPSF6*, and both strongly inhibited starvation-induced autophagosome formation (Figures 1O and 1P). Together, these results demonstrate that the CFI, CPSF, and CstF sub-complexes of the CPA complex positively regulate autophagy and that the CFII sub-complex acts negatively.

CPA Complex-Mediated APA Alters ATG1 and ATG8a Protein Expression Levels

Since the major known function of the CPA complex is 3′ end processing, we tested whether it regulates APA of *Atg* transcripts. We used 3′ RACE to identify polyadenylation sites in *Atg1* and *Atg8a* transcripts (Figures 2A, S1A, and S1B) and performed qPCR with primers that detect either total or long 3′ UTR-specific transcripts to determine 3′ UTR changes (Figure 2A). Interestingly, starvation increased 3′ UTR length of both *Atg1* and *Atg8a* transcripts, and knockdown of *CPSF6*, *Clp*, or *CstF64* reduced it (Figure 2B). In contrast, depletion of *PCF11* or *Cbc* extended 3′ UTR lengths of *Atg1* and *Atg8a* transcripts under fed conditions (Figure S1C). Thus, the CPA complex plays an important role in regulating 3′ UTR lengths of *Atg* genes.

3′ UTRs contain binding sites for microRNAs or RNA-binding proteins that affect mRNA stability, localization, or translational efficiency (Miura et al., 2014). We observed that knockdown of *CPSF6*, *Clp*, or *CstF64*, decreased *Atg1* and *Atg8a* mRNA levels, indicating that the CPA complex-dependent 3′ UTR changes of *Atg1* and *Atg8* may affect mRNA stability (Figure S1D). We therefore treated S2R+ cells with the transcriptional inhibitor actinomycin D, and measured luciferase activity and RNA levels with long or short 3′ UTRs. The half-life of luciferase mRNAs with the short *Atg1* or *Atg8a* 3′ UTRs was less than those with the long 3′ UTRs (Figure 2C), and a luciferase assay also revealed that long 3′ UTRs increase protein expression levels (Figure S1E). Consistently, depletion of *CPSF6*, *CstF64*, or *Clp*, reduced ATG1 and ATG8a protein levels in starved larval fat bodies, whereas *Cbc* or *Pcf11* knockdown increased them under fed conditions (Figures S1F and S1G). Thus, the CPA complex is required for the starvation-induced 3′ UTR elongation of *Atg1* and *Atg8a*, promoting mRNA stability and protein expression.

AS of *Atg1* Increases ATG1 Complex Formation during Starvation

Some CPA complex components regulate AS by interacting with splicing factors (Cardinale et al., 2007; Kyburz et al., 2006; Millevoi et al., 2006; Shi et al., 2009). To investigate whether the CPA complex modulates AS of *Atg1*, we examined the two major *Atg1* isoforms, *Atg1-RA* and *Atg1-RB*. *Atg1-RB* contains a translatable retained intron, spliced-out in *Atg1-RA* (Figures 2A and 2E). Levels of *Atg1-RB* slightly decreased upon starvation, but

Figure 1. The CPA Complex Regulates ATG1 and Starvation-Induced Autophagosome Formation

(A–H and A′–H′) *Atg1* genetically interacts with the CPA complex. Compared with controls (A), expression of *Atg1* using GMR-GAL4 results in a rough and reduced eye (B). *Atg1*-induced eye defects are rescued by co-expressing $Atg9^{RNAi}$ (C), $CPSF6^{RNAi}$ (D), $CstF64^{RNAi}$ (E), $WDR33^{RNAi}$ (F), or $CPSF160^{RNAi}$ (G), but enhanced by $Pcf11^{RNAi}$ (H). Third-instar larval eye imaginal discs from controls expressing *mCherry-ATG8a* alone (A′), or flies co-expressing *mCherry-Atg8a* and indicated transgenes, stained with DAPI (B′–H′).

(I) Quantification of mCherryATG8a puncta per cell in (A′–H′). One-way ANOVA followed by Bonferroni's *post hoc* test; data are represented as mean ± SEM; $^{**}p < 0.01$, $^{***}p < 0.001$.

(J–R) The CPA complex regulates autophagy. Clonal depletion of *CPSF5* (J), *CstF64* (K), or *CPSF160* (L) impaired mCherry-ATG8a puncta formation during starvation, while expression of $Pcf11^{RNAi}$ (M) or Cbc^{RNAi} (N) in GFP-nls-labeled cells induced mCherry-ATG8a puncta under fed conditions. Mutant clones of $CPSF6^{091}$ (O) or $CPSF5^{H11}$ (P), circled by dotted lines, show decreased mCherry-ATG8a puncta during starvation. Cells outside of the clones are used as controls. Fat body cells were stained with DAPI. Scale bar, 20 μm. (Q–R) Quantification of the relative number of mCherry-ATG8a dots per cell. Student's t test was performed to identify significant differences between dot numbers in clones and in control cells; data represent as the mean ± SEM of three fat-body samples per genotype; $^{*}p < 0.05$, $^{**}p < 0.01$, $^{***}p < 0.001$.

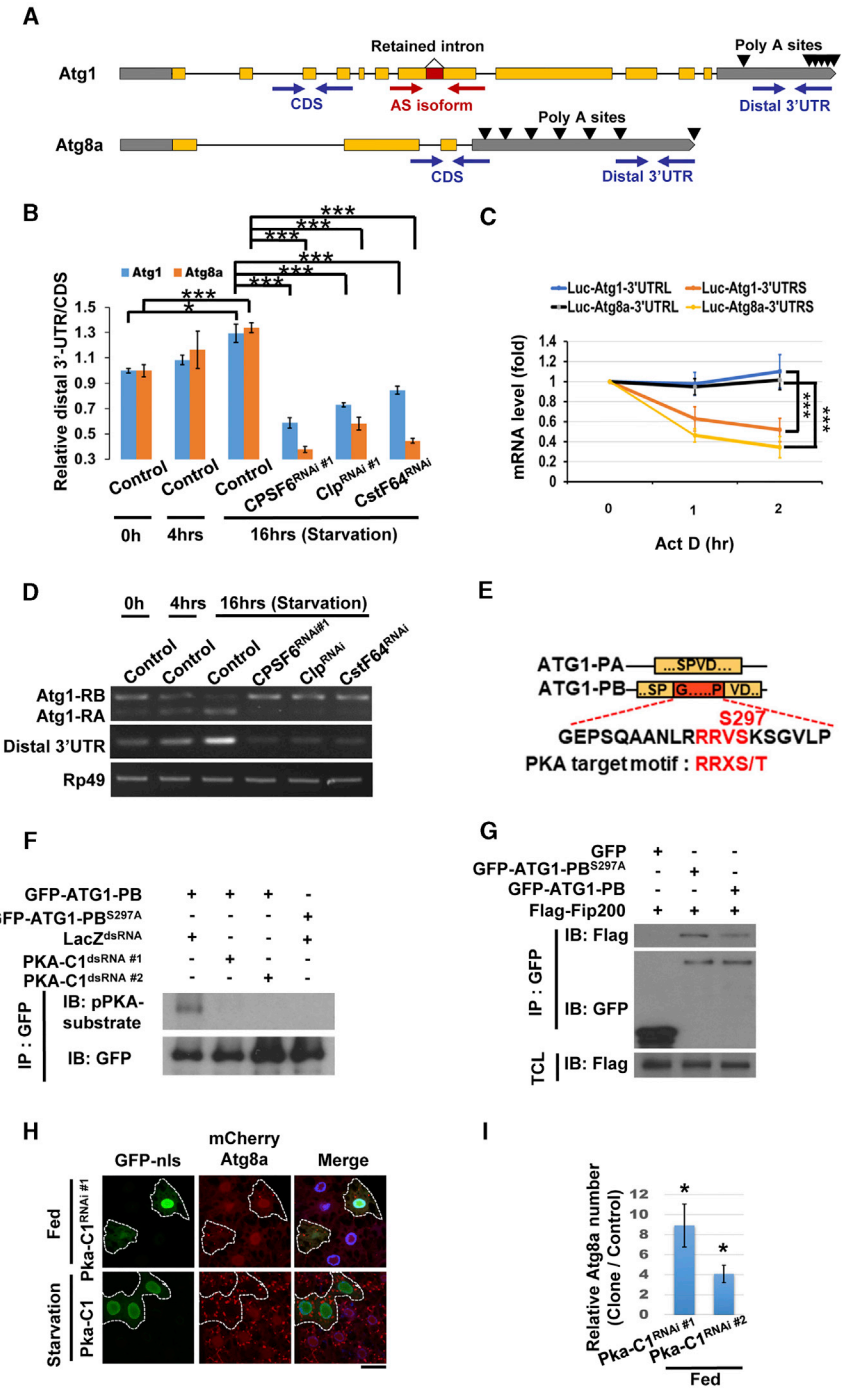

Figure 2. The CPA Complex Controls 3′ UTR Length and Splicing of *Atg1* and *Atg8a*

(A) Primers detect the *Atg1* AS isoforms (with or without the retained intron), the total (CDS), or the long specific transcripts (distal 3′ UTR) of *Atg1* and *Atg8a*. Poly(A) sites are indicated by arrows.

(B) The ratio between amplicons (distal 3′ UTR/CDS) represents APA isoform changes under different conditions. Compared with control under fed conditions (starvation 0 hr), the 3′ UTR length of *Atg1* and *Atg8a* transcripts increased in control larval fat bodies, but not from $CPSF6^{RNAi}$-, Clp^{RNAi}-, or $CstF64^{RNAi}$-expressing larva under starvation for 16 hr. One-way ANOVA followed by Bonferroni's *post hoc* test; data are represented as mean ± SEM; *p < 0.05, ***p < 0.001.

(C) Long 3′ UTRs of *Atg1* and *Atg8a* enhanced mRNA stability. *Firefly Luciferase* reporters with the indicated 3′ UTRs were transfected into S2R+ cells. After 48 hr, cells were treated with rapamycin (20 nM) for 24 hr, followed by actinomycin D (10 μg/mL) for the indicated times to measure mRNA levels of *Firefly Luciferase* by qPCR. One-way ANOVA followed by Bonferroni's *post hoc* test; data are represented as mean ± SEM; ***p < 0.001.

(D) The CPA complex mediates starvation-induced AS of *Atg1*. RNA extracted from larval fat bodies was subjected to RT-PCR to detect the two AS isoforms, *RA* and *RB*, and the long UTR-specific transcripts (distal 3′ UTR) of *Atg1*.

(E–G) PKA phosphorylates ATG1-PB-S297 to promote ATG1 kinase complex assembly. Yellow boxes represent the shared amino acid sequences between ATG1-PA and ATG1-PB, and the red box indicates the peptide sequence from the retained intron of *Atg1-RB*. Alignment of amino acid sequences encoded by the retained intron of *Atg1-RB* showing the PKA phosphorylation motif (E). S2R+ cells were treated with dsRNA against *LacZ* or *PKA-C1*. After 48 hr, cells were transfected with *GFP-Atg1-RB* or *GFP-Atg1-RB*^{S297A}, and then subjected to immunoprecipitation (IP), followed by immunoblotting (IB) with antibodies as indicated (F). S2R+ cells transfected with plasmids as indicated were subjected to IP. Immunoprecipitated proteins and total cell lysates (TCL) were analyzed by IB with antibodies as indicated (G).

(H) Clonal expression of $PKA\text{-}C1^{RNAi}$ in GFP-nls-labeled cells increased mCherry-ATG8a puncta under fed conditions, but *PKA-C1* expression failed to affect it upon starvation (H). Cells outside of the clones are used as controls. Fat body cells are stained with DAPI. Scale bar, 20 μm.

(I) Quantification of the relative number of mCherry-ATG8a dots. Student's t test was performed to identify significant differences between dot numbers in clones and in control cells; data are represented as mean ± SEM of three fat-body samples per genotype; *p < 0.05.

Atg1-RA was increased (Figure 2D). This phenomenon was blocked by reduction of *CPSF6*, *Clp*, or *CstF64* expression (Figure 2D). In contrast, depletion of *Pcf11* or *Cbc* increased *Atg1-RA* levels under fed conditions (Figure S1H), suggesting that the CPA complex regulates AS of *Atg1* upon starvation.

To identify the splicing factors influencing *Atg1* intron retention, we tested those that associate with the CPA complex in mammalian cells (Cardinale et al., 2007; Kyburz et al., 2006; Millevoi et al., 2006; Shi et al., 2009). Depletion of *9G8* triggered mCherry-ATG8a puncta formation and increased *Atg1-RA* under fed conditions, while *9G8* overexpression reduced starvation-induced ATG8a punctae and blocked AS of *Atg1* triggered by *Cbc* depletion (Figures S1I–S1K and S1P). Depletion of U2AF50 suppressed starvation-induced autophagy and

Cbc-RNAi-induced AS of *Atg1* (Figures S1I, S1O, and S1P). In contrast, depletion of *SRm300*, *Rbp1-like*, and *Tra2*, did not affect mCherry-ATG8a punctae formation (Figures S1L–S1N and S1P). We further noted that changes in the *Atg1* 3′ UTR correlate with *Atg1* isoform alteration (Figures 2D and S1H). Thus, APA and AS of *Atg1* are coordinately regulated by the CPA complex and splicing factors, including 9G8 and U2AF50.

As the *Atg1*-retained intron was largely removed by splicing during starvation, we tested whether it contained sequences important for ATG1 regulation. The peptide sequence encoded by the retained intron of *Atg1-RB* contains a PKA consensus phosphorylation site (RRXS*) at Ser-297 (Figure 2E) (Smith et al., 2011). PKA phosphorylates and inhibits ATG1 in yeast and mammalian cells (Budovskaya et al., 2005; Dorsey et al., 2009; Stephan et al., 2009). To test whether PKA phosphorylates ATG1-PB Ser-297, we examined its phosphorylation using phospho-PKA substrate antibody in S2R+ cells. Immunoblotting of anti-GFP immunoprecipitates revealed that GFP-ATG1-PB was phosphorylated and that the phosphorylation signal was abolished after knocking down PKA expression or mutating Ser-297 (Figure 2F). We performed *in vitro* kinase assays to further test whether a S297A mutation in ATG1-PB affects ATG1 kinase activity using wild-type ATG1-PB or ATG1-PB-S297A isolated from S2R+ transfected cells as kinases, and myelin basic protein as a substrate. The S297A mutation had no significant effect on ATG1-PB kinase activity (data not shown), consistent with a study showing that PKA regulates the association of ATG1 with the preautophagosomal structure, but not its protein kinase activity (Budovskaya et al., 2005). In contrast, co-immunoprecipitation revealed that the S297A mutation enhanced the interaction between ATG1-PB and FIP200, a component of the ATG1 complex (Figure 2G). Furthermore, wild-type ATG1 and ATG1S297A transgenic flies revealed that the mutant protein induces higher autophagic activity than wild-type (Figures S1Q–S1S). Thus, PKA-mediated phosphorylation of ATG1-PB blocks ATG1 complex assembly to inhibit autophagy initiation. Moreover, depletion of *PKA*-induced mCherry-ATG8a punctae formation in larval fat body from fed larvae, but had no effect on starvation-induced autophagy, while *PKA* overexpression failed to inhibit autophagy upon starvation (Figures 2H and 2I; data not shown). These results demonstrate that PKA inhibits ATG1 protein complex formation to repress autophagy by phosphorylating ATG1-PB Ser-297 under fed conditions. Upon starvation, removal of the retained intron in *Atg1* transcripts bypasses PKA negative regulation of ATG1, enhancing autophagy.

TORC1 Signaling Regulates *Atg* mRNA Processing and CPSF6 Phosphorylation

TORC1 signaling pathway regulates aspects of APA and AS (Chang et al., 2015; Lee et al., 2017). Thus, we tested whether TORC1 activity regulates CPA complex-mediated mRNA processing. Tsc1/2 overexpression, which blocks TORC1 activity, increased mCherry-ATG8a punctae and reduced cell size in the larval fat body (Figures 3A and 3E). *CPSF6-RNAi*, *CPSF160-RNAi*, or *CstF64-RNAi*, inhibited the TSC1/2-induced effects (Figures 3B–3D and 3E), suggesting that the CPA complex functions as a downstream target of TORC1 signaling in the modulation of autophagy.

Next, we tested whether TORC1 signaling affects mRNA processing during nutrient deprivation. RT-PCR and qPCR data indicate that expression of *PI3K92E*, *Pten-RNAi*, *myr-AKT*, *Tsc1-RNAi*, or wild-type *TOR* (TOR^{wt}) blocked starvation-induced 3′ UTR elongation of *Atg1* and *Atg8a*, as well as *Atg1* isoform conversion (Figures 3F and 3G). Conversely, inhibition of TORC1 activity by expressing *InR-RNAi*, *PI3K92E-RNAi*, *Pten*, *PDK1-RNAi*, *Rheb-RNAi*, or *TOR-RNAi* under fed conditions phenocopied starvation-induced RNA processing, suggesting that TORC1 controls mRNA processing of *Atg1* and *Atg8*, possibly through the CPA complex (Figures S2A and S2B).

We expressed GFP-tagged components of the CPA complex in S2R+ cells and then used anti-phospho-Ser and -Thr antibody to determine their phosphorylation. Immunoblotting of anti-GFP immunoprecipitates revealed that both CstF64 and CPSF6 were phosphorylated, but only CPSF6 phosphorylation was increased by the TOR inhibitor rapamycin (Figures 3H and S2C). Furthermore, CPSF6 phosphorylation was reduced in *TSC1* or *TSC2* knockout mutant cells, indicating that TORC1 activity negatively regulates CPSF6 phosphorylation (Figure S2D).

CDK8 and *DOA* Genetically Interact with *TOR* and *CPSF6*

Studies in yeast and mammalian cells show that TORC1 reduces the protein levels of CDK8 and KNS1, DOA orthologs in yeast (Feng et al., 2015; Lee et al., 2012). Moreover, high-throughput affinity purification and mass spectrometry (MS) and yeast two-hybrid analyses suggest that CDK8 and CLK2 (DOA ortholog in mammals) interact with many CPA components (Guruharsha et al., 2011; Rolland et al., 2014; Varjosalo et al., 2013), suggesting that these kinases might link TORC1 and CPSF6. We therefore tested whether these components genetically interact. Both *TSC1/2* overexpression-induced autophagy and reduction of cell size were suppressed by depletion of *CDK8*, *DOA*, or *CycC*, the binding partner of CDK8, suggesting that CDK8/CycC and DOA function downstream of TORC1 (Figures 4A–4D and 4I). Moreover, overexpression of *CDK8* or *DOA* triggers autophagy under fed conditions, and their phenotypes were inhibited by *CPSF6* depletion (Figures 4E–4H and 4J). Interestingly, we found that *CycC-RNAi* or *DOA-RNAi* represses DOA- or CDK8-induced autophagy, respectively, and that CDK8 and DOA associate with each other under rapamycin treatment (Figures S3A–S3C), suggesting that they form a complex. Thus, these results establish TORC1-CDK8/DOA-CPA as a new signaling pathway that regulates autophagy.

CPSF6 Is a Substrate of CDK8 and DOA Kinases that Are Negatively Regulated by TORC1

We investigated the mechanism of TORC1-dependent regulation of CDK8 and DOA. CDK8 and DOA protein levels were increased in S2R+ cells treated with rapamycin (Figure S3D). Importantly, ubiquitination of CDK8 and DOA was increased by MG132, a proteasome inhibitor, and rapamycin co-treatment reduced it, indicating that TORC1 negatively regulates CDK8 and DOA via ubiquitin-mediated degradation (Figure S3E).

Next, we investigated whether CPSF6 physically interacts with CDK8 or DOA. CPSF6 is a Ser/Arg-rich (SR)-like protein that contains sequences rich in Arg-Ser and/or Arg-Asp/Glu/Gly dipeptides (referred to as the RS domain) (Figure 4K). S2R+ cells

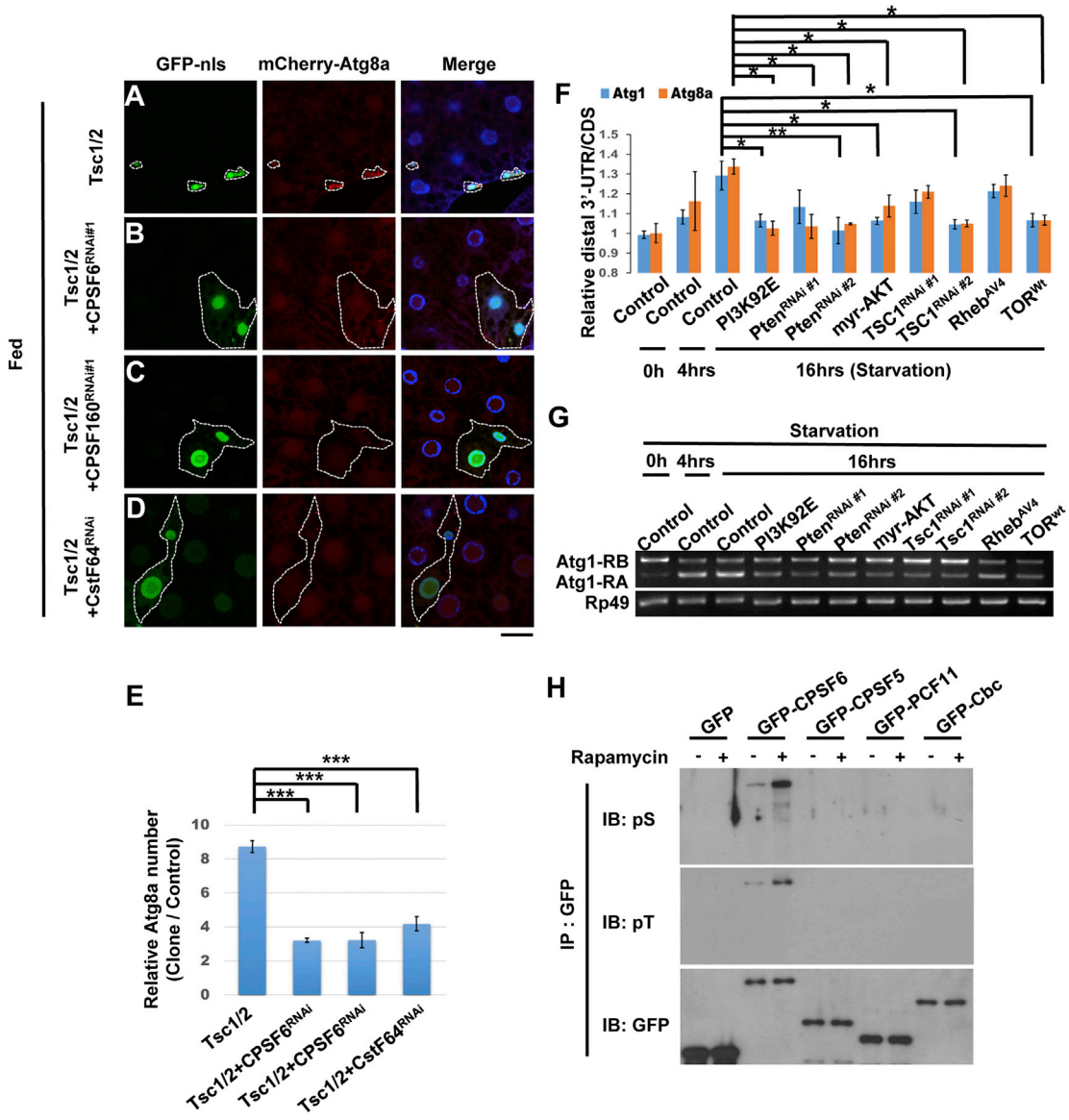

Figure 3. TORC1 Signaling Regulates the CPA Complex by Inhibiting CPSF6 Phosphorylation

(A–E) The CPA complex genetically interacts with *TOR*. Clonal expression of *TSC1* and *TSC2* reduced cell size and increased mCherry-ATG8a puncta in the larval fat body under fed conditions (A). These effects were suppressed by depletion of *CPSF6* (B), *CPSF160* (C), or *CstF64* (D). Fat body cells were stained with DAPI. Scale bar, 20 μm. Quantification of the relative number of mCherry-ATG8a dots per cell. One-way ANOVA followed by Bonferroni's *post hoc* test; data are represented as mean ± SEM; ***p < 0.001 (E).

(F and G) PI3K/AKT/TORC1 signaling regulates APA and AS of *Atg1* and *Atg8a*. RNA from larval fat body of indicated transgenes was subjected to qPCR or RT-PCR to detect APA and AS isoforms. One-way ANOVA followed by Bonferroni's *post hoc* test; data are represented as mean ± SEM; *p < 0.05, **p < 0.01.

(H) Rapamycin enhances phosphorylation of CPSF6. S2R+ cells transfected with plasmids as indicated were treated with or without rapamycin (20 nM) for 24 hr and then subjected to IP, followed by IB.

were transfected with *GFP-CPSF6*, together with *Flag-CDK8* or *HA-DOA*, and then treated with or without rapamycin. Immunoblotting of anti-GFP immunoprecipitates revealed that CPSF6 co-precipitated with CDK8 and DOA following rapamycin treatment (Figures S3G and S3H). However, CPSF6 carrying a deletion in the RS domain (CPSF6ΔRS) did not interact with either CDK8 or DOA (Figures S3F–S3H), suggesting that CDK8 and DOA interact with CPSF6 through its RS domain when TORC1 is inactivated.

Many RNA-processing proteins possess RS-domains that are extensively phosphorylated, and it is the overall charge of the phosphorylated RS domain that determines their structure and activities (Ghosh and Adams, 2011; Xiang et al., 2013). The primary sequence of the CPSF6 RS-domain reveals a total of 37 serine and threonine residues, of which 12 match DOA consensus phosphorylation sites and 2 match CDK8 consensus phosphorylation sites (Figure S4A). Thus, we investigated whether CDK8 and DOA are responsible for rapamycin-induced

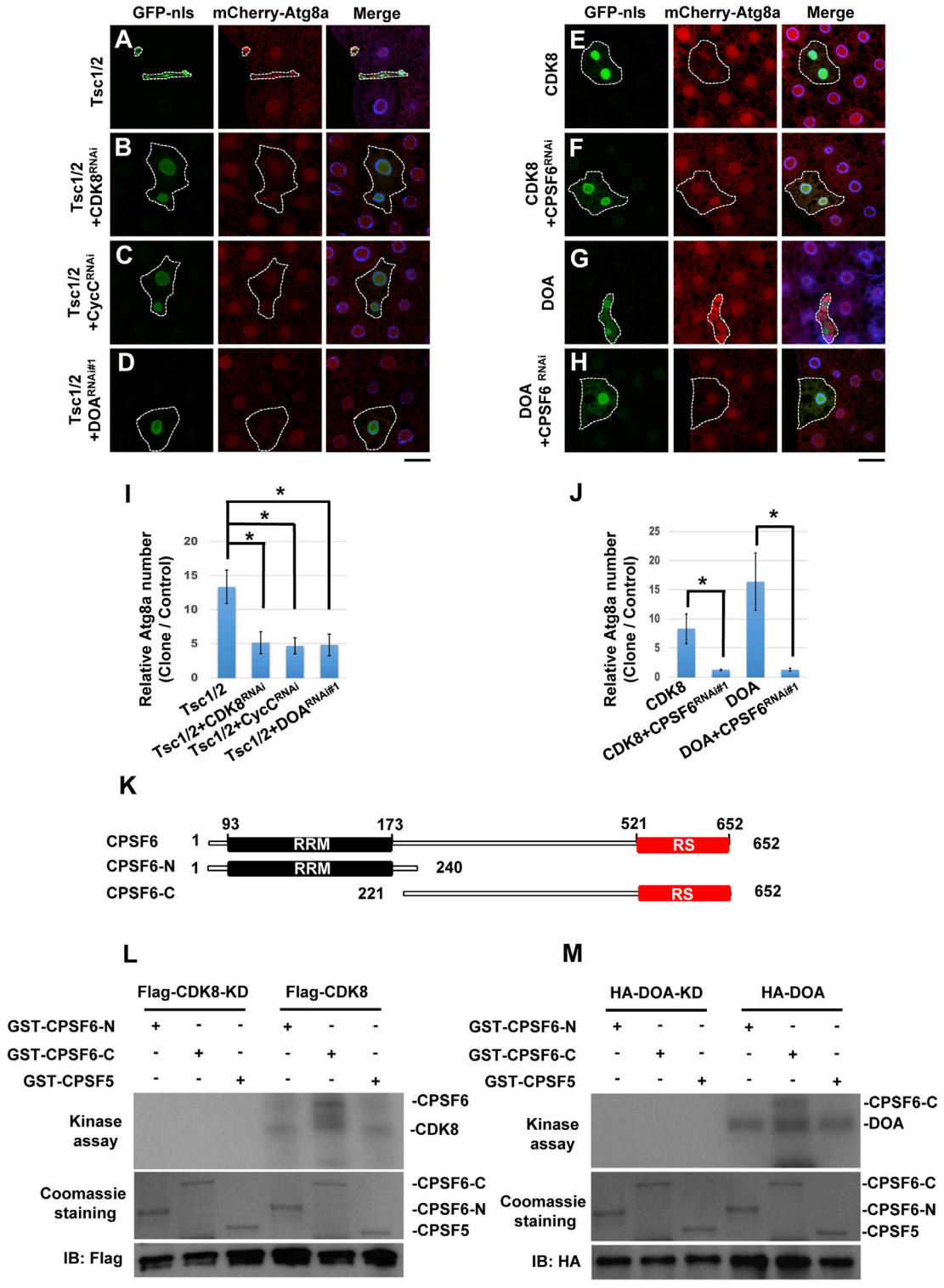

Figure 4. Genetic and Biochemical Interactions between TOR, CDK8/CycC, DOA, and CPSF6

(A–K) Genetic interactions between *TOR*, *CDK8*/*CycC*, *DOA*, and *CPSF6*. Clonal expression of *TSC1* and *TSC2* reduced cell size and increased mCherry-ATG8a puncta formation in the larval fat body under fed condition (A), and these effects were suppressed by depletion of *CDK8* (B), *CycC* (C), or *DOA* (D). Clonal expression of *CDK8* (E) or *DOA* (G) induced mCherry-ATG8a puncta formation under fed conditions, and depletion of *CPSF6* inhibits the *CDK8*- or *DOA*-induced effects (F and H). Fat body cells were stained with DAPI. Scale bar, 20 μm. (I and J) Quantification of the relative number of mCherry-ATG8a dots per cell. One-way

(legend continued on next page)

phosphorylation of CPSF6. Label-free quantitative MS identified two phosphorylation sites at Ser-588 (a potential DOA phosphorylation site) and Ser-596 (a potential CDK8 phosphorylation site) in a peptide corresponding to residues 585–613 of CPSF6. Both of their phosphorylation levels increased after rapamycin treatment (Figure S4B). Depletion of either *CDK8* or *DOA* reduced the rapamycin-induced phosphorylation of CPSF6, indicating that CDK8 and DOA promote CPSF6 phosphorylation as TORC1 is inhibited (Figure S4C). Finally, we performed *in vitro* kinase assays to test whether CPSF6 is a substrate of CDK8 and DOA using CDK8 and DOA isolated from transfected cells, and recombinant CPSF6 proteins as substrates. CDK8 and DOA both phosphorylated the C-terminal region of CPSF6, CPSF6-C (amino acids 221–652), but not its N-terminal region, CPSF6-N (amino acids 1–240), or CPSF5 (Figures 4K–4M). We further determined the CPSF6 phosphorylation sites of DOA and CDK8 using *in vitro* kinase assays followed by MS. Tandem MS analyses demonstrate that CPSF6-S588 is directly phosphorylated by DOA, and CPSF6-S596 is phosphorylated by CDK8 (Figure S4A). Together, these data indicate that CDK8 and DOA directly phosphorylate the RS domain of CPSF6.

RS Domain Phosphorylation of CPSF6 Is Required for Its Nuclear Localization, RNA Binding, and Starvation-Induced RNA Processing and Autophagy

The RS domain of CPSF6 largely contributes to its nuclear localization and to the RNA-binding ability of the CFI sub-complex (Dettwiler et al., 2004). We thus tested whether CPSF6 with mutations of all 14 phosphorylatable sites to alanine ($CPSF6^{14A}$) or CPSF6 carrying a deletion of the RS domain ($CPSF6^{\Delta RS}$) affected its sub-cellular localization and ability to associate with RNA. $CPSF6^{14A}$ and $CPSF6^{\Delta RS}$ exhibited decreased phosphorylation signal even after rapamycin treatment (Figure S4C). We found that GFP-CPSF6 was enriched in the nuclei of S2R+ cells with or without rapamycin treatment, indicating that the basal level of CPSF6 phosphorylation is sufficient to induce its nuclear localization (Figures 5A and 5B). However, CPSF6 redistributed to the cytoplasm in *TSC1* or *TSC2* knockout cells, and this was reversible by rapamycin (Figure S4D). Ablation of either *CDK8* or *DOA* also resulted in cytoplasmic localization of CPSF6 (Figures 5C–5F). $CPSF6^{14A}$ or $CPSF6^{\Delta RS}$ were also cytoplasmic (Figures 5G and 5H), suggesting that phosphorylation of the CPSF6 RS domain controls its nuclear localization.

RNA immunoprecipitation revealed that CPSF6 co-precipitated with *Atg1* and *Atg8a* transcripts and that these interactions were enhanced by rapamycin (Figure 5I). Conversely, the interaction between CPSF6 and *Atg* transcripts was suppressed in *TSC1* or *TSC2* knockout cells and this effect was reversed by rapamycin, suggesting that TORC1 activity regulates the RNA binding ability of CPSF6 (Figure S4E). *CDK8* or *DOA* depletion abolished binding of CPSF6 to *Atg* transcripts under rapamycin treatment, and $CPSF6^{14A}$ or $CPSF6^{\Delta RS}$ also exhibited reduced RNA binding (Figure 5I). Thus, CDK8- and DOA-mediated phosphorylation of the CPSF6 RS domain is required not only for its nuclear localization but also for RNA binding.

We further tested the *in vivo* function of CPSF6 phosphorylation on regulating starvation-induced RNA processing and autophagosome formation. Starvation-induced *Atg1* and *Atg8a* 3′ UTR extensions and *Atg1* isoform conversion were repressed in the larval fat body of *CDK8* mutant, *DOA* mutant, $CPSF6^{14A}$-, or $CPSF6^{\Delta RS}$-expressing flies (Figures 5J, 5K, S4F, and S4G). In addition, *CDK8* or *DOA* mutations decreased ATG1 and ATG8a protein levels (Figure S4H). Likewise, overexpression of $CPSF6^{14A}$ or $CPSF6^{\Delta RS}$ reduced ATG1 and ATG8a protein levels (Figure S4I). Finally, starvation-induced ATG8a punctae formation was blocked by *CDK8-RNAi*, *DOA-RNAi*, $CPSF6^{14A}$, or $CPSF6^{\Delta RS}$ (Figures 5L–5P), confirming that CDK8- and DOA-mediated CPSF6 phosphorylation is required for RNA processing of *Atg* transcripts and autophagy upon nutrient deprivation.

The CDK8/DOA/CPA Axis Regulates Lipid, Protein, and Energy Metabolism

Besides inhibiting autophagy, TORC1 promotes protein synthesis, lipogenesis, and energy metabolism (Saxton and Sabatini, 2017). To test whether CDK8/DOA/CPA signaling mediates other physiological effects of TORC1, we performed global transcriptomic analysis of wild-type or *CPSF5* mutant larval fat bodies under fed or starvation conditions. CFSF5 and CPSF6 are constitutive components of the CFI sub-complex, and knockdown of either CPSF5 or CPSF6 results in preferential use of proximal polyadenylation sites in mammalian cells (Martin et al., 2012). Because *CPSF6* mutants mostly die during the first larval instar, we examined *CPSF5* mutants as they survive to third instar and exhibit phenotypes similar to *CPSF6* mutants (Figures 1O, 1P, 5J, 5K, and S4I).

Gene set enrichment analysis demonstrated that biosynthetic processes were downregulated during starvation, while many stress responses were upregulated (Figures 6A and S5A–S5E). Comparison of the transcriptome changes in the fat body of 16-hr-starved larvae versus starved *CPSF5* mutant larvae revealed that 585 of 1,933 differentially expressed genes responding to starvation were CPSF5 dependent (Figure 6A; Table S2). Gene set enrichment analyses further suggest that autophagy, changes of lipid, protein, and energy metabolism, but not chromosome organization or intracellular transport, are regulated by CPSF5 (Figures 6A and S5A–S5E). These CPSF5-dependent genes were further visualized by generating a protein-protein interaction network (Figure 6B). We also used COMPLEAT (Hu et al., 2017) to perform a protein complex-enrichment analysis and identify several protein complexes required for autophagy and nutrient and energy metabolism (Figure S5F). These analyses indicate that the CPA complex is involved in starvation-induced metabolic changes.

qPCR confirmed that the expression of multiple genes involved in glycolysis, translation, and energy metabolism was

ANOVA followed by Bonferroni's *post hoc* test; data are represented as mean ± SEM; *$p < 0.05$. (K) Schematic representation of the domain structures of CPSF6 and deletion mutants.

(L and M) CDK8 and DOA directly phosphorylate CPSF6 *in vitro*. Flag-CDK8, CDK8-KD (L), HA-DOA, or HA-DOA-KD (kinase-dead) (M) immunoprecipitated from lysates of transfected cells were used to phosphorylate bacterially expressed recombinant CPSF6-N, CPSF6-C, and CPSF5 in an *in vitro* kinase assay. Lower panels demonstrate the equal input of GST-fusion proteins and CDK8 or DOA immunoprecipitates.

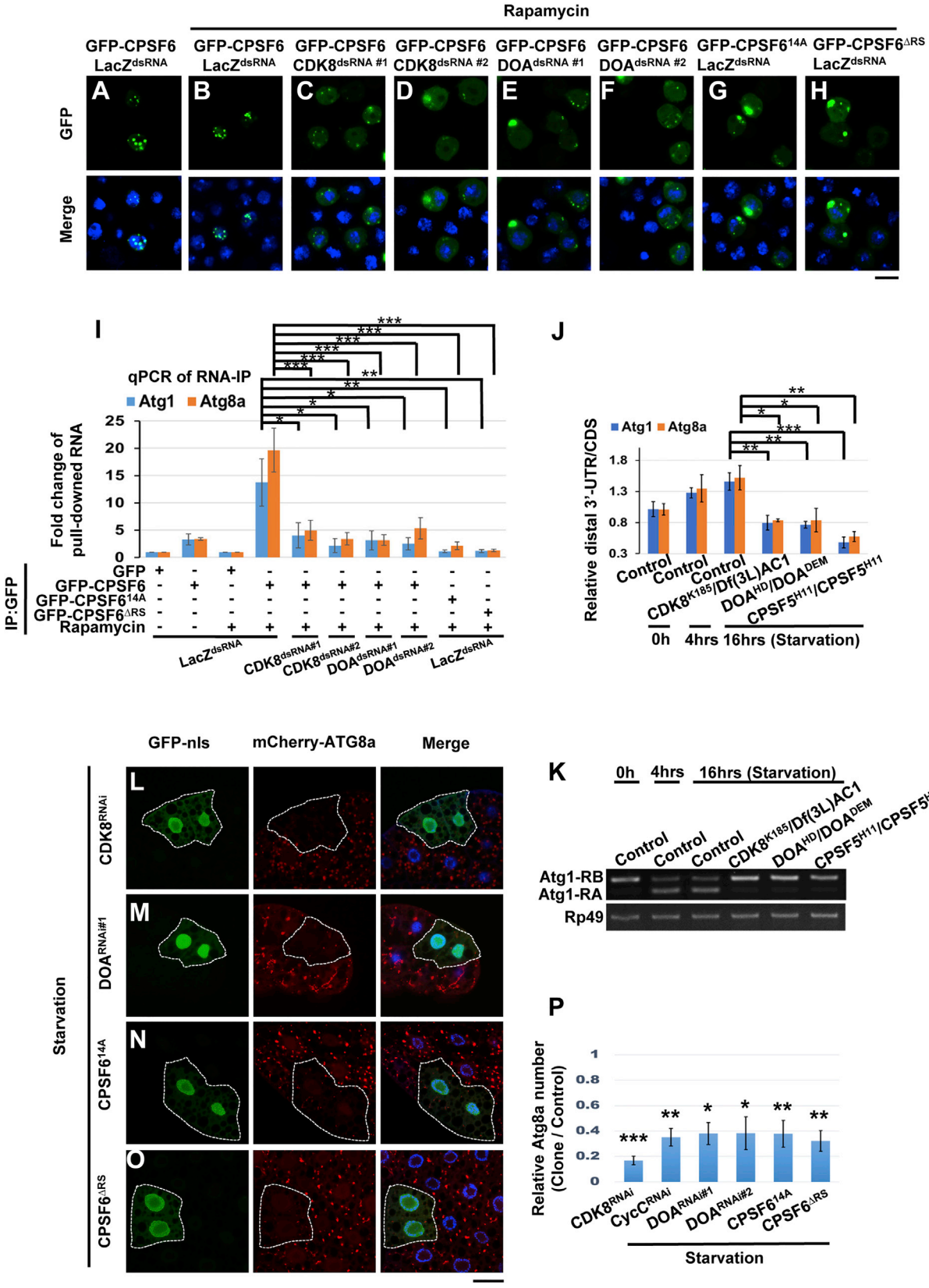

(legend on next page)

enhanced in the fat body of *Tsc2*, *CDK8*, *DOA*, and *CPSF5* mutant starved larvae, compared with wild-type starved larvae (Figure S5G). In contrast, the expression of genes involved in autophagy and lipid digestion was significantly reduced in *Tsc2*, *CDK8*, *DOA*, or *CPSF5* mutants (Figure S5G). Furthermore, many metabolic genes exhibited starvation-induced APA in a *Tsc2*/*CDK8*/*DOA*/*CPA*-dependent manner (Figure 6C). We also found strong correlation of CPSF5 dependency with genes that are alternatively spliced among metabolic genes (Figure 6D; Table S3), indicating that the CDK8/DOA/CPA complex regulates AS and APA of metabolic genes during starvation.

To investigate the role of the CDK8/DOA/CPA complex in the regulation of metabolism, we measured triglyceride (TAG), protein, and ATP levels in whole larvae. Compared with fed conditions, starvation reduced TAG, protein, and ATP levels, but these nutrient levels were increased in *CDK8*, *DOA*, or *CPSF5* mutants (Figure 6E). Nile red staining for monitoring lipid droplets in the larval fat body confirmed that depletion of *CDK8*, *DOA*, or *CPSF6* enhanced lipid storage (Figure S5H). These results demonstrate that CDK8/DOA/CPA regulate autophagy, as well as lipid, protein, and energy metabolism.

CDK8/CLK2/CPSF6 Are Essential for Metabolic Reprogramming during Starvation in Mammalian Cells

The role of the CPA complex in regulating 3′ UTR lengths was reported in mammalian cells (Martin et al., 2012). To investigate whether the CDK8/DOA/CPSF6 pathway is conserved in mammals, we tested whether CPSF6, CDK8, and CLK2, the closest human ortholog of DOA among CLK kinases, interact. Consistent with our observations in *Drosophila*, co-immunoprecipitations revealed that CPSF6 physically interacts with CDK8 and CLK2 during starvation (Figure S6A). In addition, *in vitro* kinase assays showed that CDK8 and CLK2 directly phosphorylate the RS domain of human CPSF6 (Figures 7A–7C). Furthermore, treatment of cells with Senexin A (a CDK8 inhibitor) or TG003 (a CLK kinase inhibitor) abrogate starvation-induced CPSF6 phosphorylation, its nuclear localization, and RNA-binding ability (Figures S6B–S6D). These results demonstrate the evolutionarily conserved roles of human CDK8 and CLK2 in the regulation of CPSF6.

We further investigated the roles of CDK8/CLK2/CPSF6 in regulating starvation-induced autophagy and metabolic changes. MCF7 cells transfected with *CPSF6* small hairpin RNA or treated with Senexin A or TG003 were incubated in a starvation medium (EBSS) in the presence or absence of the lysosomal inhibitor bafilomycin A1 (BafA1). Depletion of CPSF6, or inactivation of CDK8 or CLK2, reduced LC3 puncta and suppressed the conversion of cytosolic LC3 (LC3-I) to the lipidated form of LC3 (LC3-II) (Figures 7D, 7E, S6E, and S6F). Moreover, depletion of CPSF6 or inhibition of CDK8 or CLK2 increased TAG, protein, and ATP levels (Figures 7F and 7G). Thus, the roles of CPSF6, CDK8, and CLK2 in the control of autophagy, lipid, protein, and energy metabolism, are conserved from flies to mammals.

DISCUSSION

In this study, we found that the CPA complex acts as a downstream effector of TORC1 signaling to regulate AS and APA, affecting protein levels and functions. CDK8 and DOA are inhibited by TORC1-dependent ubiquitination and phosphorylate CPSF6. Phosphorylated CPSF6 translocates to the nucleus and induces alternative RNA processing of transcripts involved in autophagy and metabolism. Depletion of CDK8, DOA, or the CPA complex compromises autophagy and promotes altered metabolism during nutrient deprivation. Importantly, the functions of CDK8, DOA/CLK2, and CPSF6 are conserved in mammals (Figure S7).

CPA Complex-Regulated AS and APA Control Autophagy

APA and AS are prevalent RNA processing events that regulate mRNA turnover (Miura et al., 2014) and generate different protein isoforms (Chabot and Shkreta, 2016). We found that the CPA complex and two splicing factors, 9G8 and U2AF50, control AS and APA of *Atg* transcripts. However, we were unable to identify global 3′ UTR changes by SUPPA (Alamancos et al., 2015) or using the APA analysis method (Chang et al., 2015). Using qPCR to detect long UTR-specific transcripts provides an alternative method to examine 3′ UTR changes of individual genes. However, in some cases, primer designs can be problematic as it is difficult to design optimal primers to detect transcripts with very short 3′ UTRs or 3′ UTRs that overlap with other genes.

RegRNA, a web server for identifying functional RNA motifs and sites, predicts a stem-loop structure in the long 3′ UTR, but not in the short 3′ UTR of *Atg1* (Chang et al., 2013a). Stem-loop structures direct RNA folding or protect mRNAs from

Figure 5. Phosphorylation of the RS Domain of CPSF6 Is Required for Its Nuclear Localization, Binding to RNA, and Autophagy

(A–H) Phosphorylation of the RS domain of CPSF6 is required for its nuclear localization. S2R+ cells were treated as in Figure S4C and then subjected to immunofluorescence. GFP-CPSF6 was localized in the nuclei of control cells ($LacZ^{dsRNA}$) with or without rapamycin (20 nM) (A and B), whereas it redistributed to the cytoplasm in cells treated with dsRNAs against *CDK8* or *DOA* (C–F). GFP-$CPSF6^{14A}$ and GFP-$CPSF6^{\Delta RS}$ were localized in the cytoplasm (G and H). S2R+ cells are stained with DAPI (blue). Scale bar, 10 mm.

(I) Phosphorylation of the RS domain of CPSF6 is critical for RNA binding. Cells as in Figure S4C were subjected to RNA immunoprecipitations, followed by qRT-PCR with primers (Figure 2A), which detect total transcript (CDS) of *Atg1* or *Atg8a*. Plotted fold-change values (ratios of RNA IP/input normalized to GFP control) are the mean ± SEM of triplicates. One-way ANOVA followed by Bonferroni's *post hoc* test; data are represented as mean ± SEM; $^{*}p < 0.05$, $^{**}p < 0.01$, $^{***}p < 0.001$.

(J and K) CDK8 and DOA affected APA and AS of *Atg1* and *Atg8a* transcripts. RNA extracts from larval fat body in control or mutants as indicated were subjected to qPCR (J) or RT-PCR (K) analysis to detect the APA and AS isoforms of *Atg1* and *Atg8a*. One-way ANOVA followed by Bonferroni's *post hoc* test. Data are represented as mean ± SEM; $^{*}p < 0.05$, $^{**}p < 0.01$, $^{***}p < 0.001$.

(L–P) CDK8- and DOA-mediated CPSF6 phosphorylation is required for autophagosome formation. Clonal expression of indicated transgenes (L–O) in GFP-nls-labeled cells reduced mCherry-ATG8a puncta upon starvation. Cells outside the clones are used as controls. Fat body cells were stained with DAPI. Scale bar, 20 μm. (P) Quantification of the relative number of mCherry-ATG8a dots per cell. Student's t test was performed to identify significant differences between dot numbers in clones and in control cells; data represent as the mean ± SEM of three fat-body samples imaged per genotype; $^{*}p < 0.05$, $^{**}p < 0.01$, $^{***}p < 0.001$.

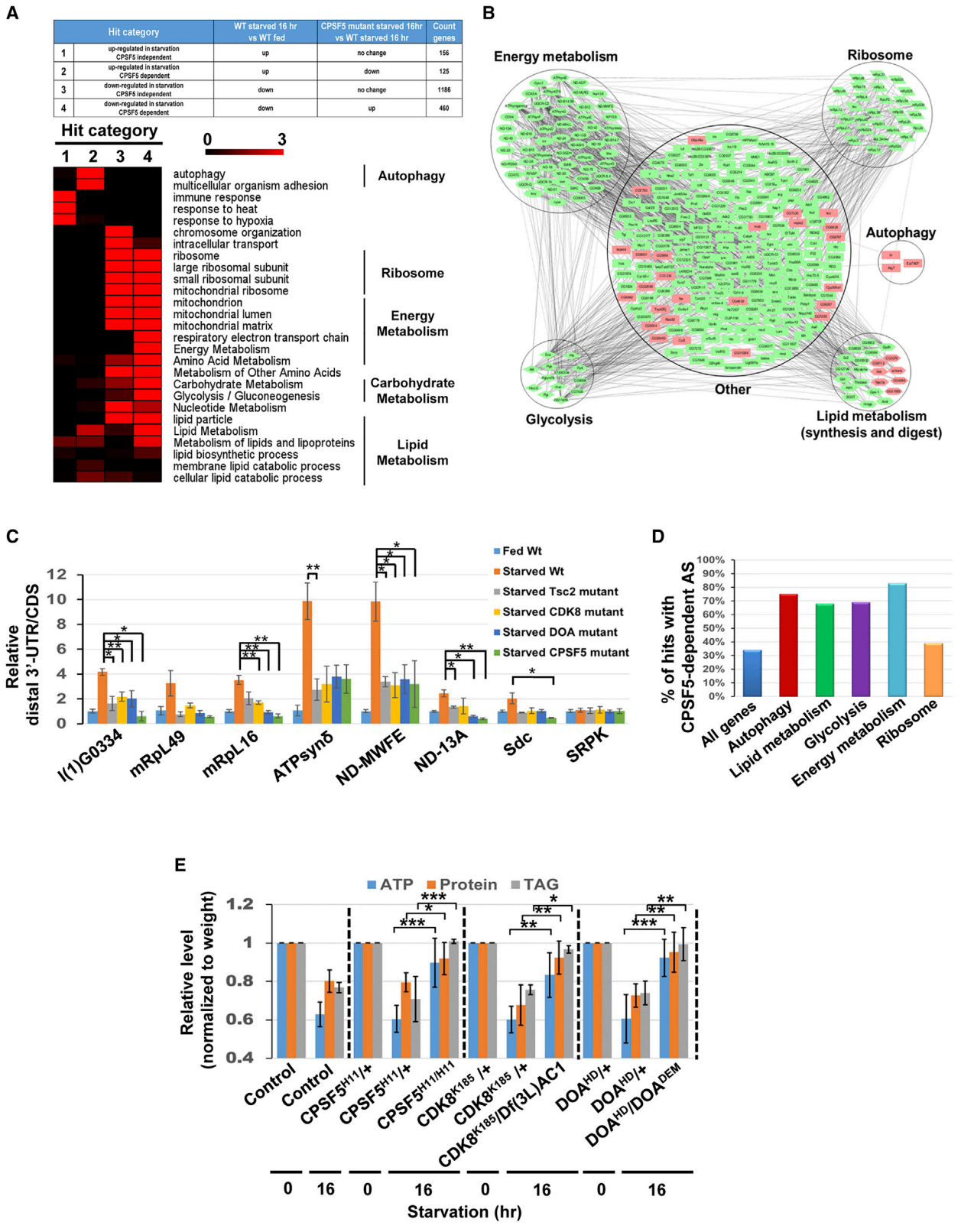

Figure 6. The CDK8/DOA/CPA Complex Controls Lipid, Protein, and Energy Metabolism

(A and B) RNA sequencing analysis of transcriptome changes in the fat body of fed larvae, 16-hr-starved larvae, and 16-hr-starved *CPSF5* mutant larvae. Heatmap displaying the -$\log_{10}$ (p value) for each gene ontology term. Color represents strength of significance (A). Network presentation of gene set enrichment

(legend continued on next page)

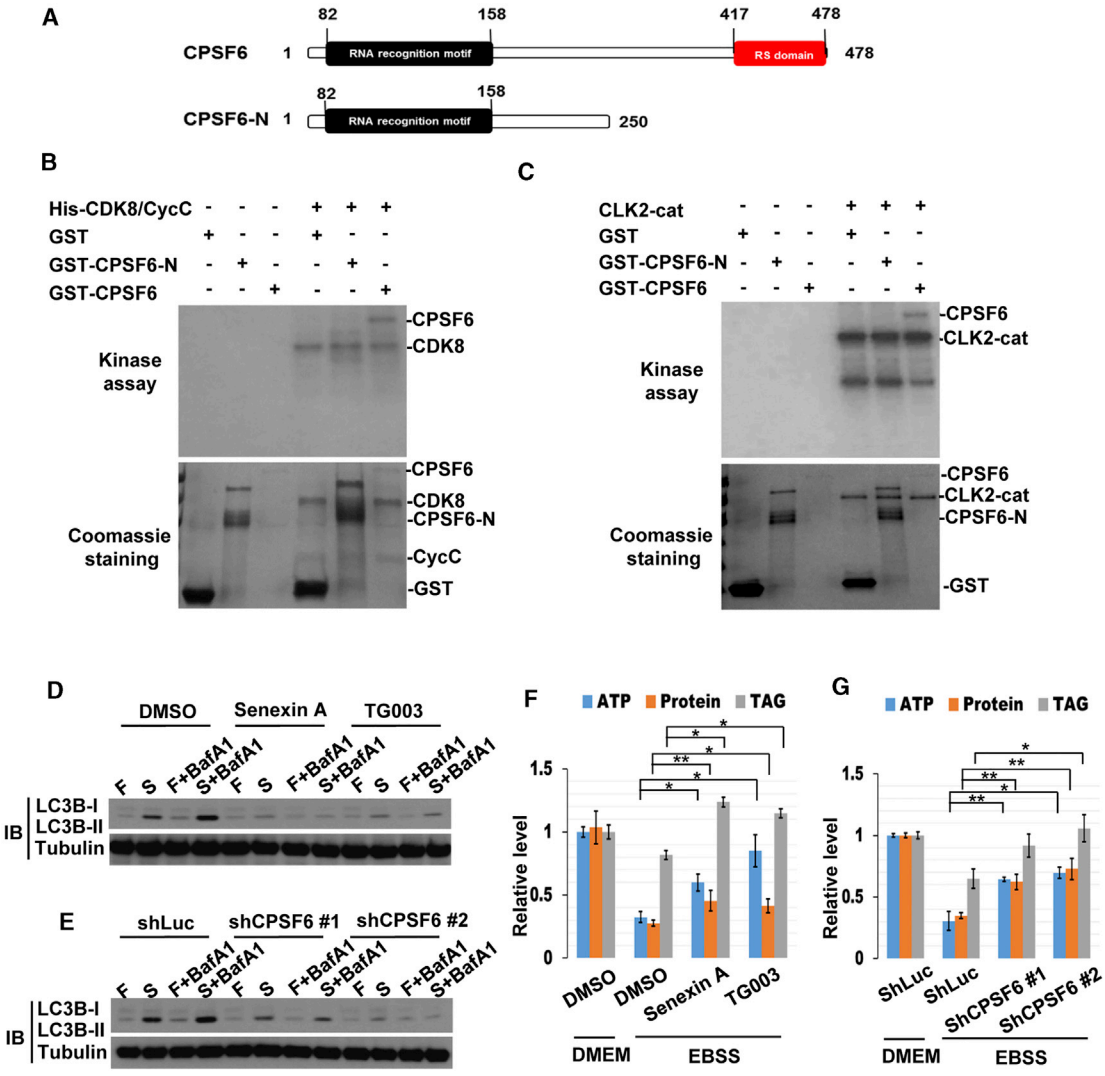

Figure 7. CDK8/CLK2/CPSF6 Regulate Autophagy and Metabolism in Mammalian Cells

(A) Schematic representation of the domain structures of human CPSF6 and the C-terminal deletion mutant (CPSF6-N).

(B and C) CDK8 and CLK2 directly phosphorylate human CPSF6 *in vitro*. Recombinant His-CDK8/CycC (B) or CLK2 catalytic domain (CLK2-cat) (C) was used to phosphorylate recombinant CPSF6 or CPSF6-N. The lower panels represent the amounts of recombinant proteins.

(D–G) CDK8/CLK2/CPSF6 are required for autophagy and metabolomic changes during starvation. MCF7 cells, treated with 50 μM Senexin-A (CDK8 inhibitor) or 50 μM TG003 (CLK2 inhibitor) (D and F) or infected with lentivirus expressing control (shLuc) or CPSF6 small hairpin RNA (E and G), were cultured in DMEM (fed) or EBSS (starvation) with or without bafilomycin A1 (BafA1) for 2 hr, and immunoblotted with antibodies as indicated (D and E) or subjected to ATP, protein, and TAG analysis (F and G). One-way ANOVA followed by Bonferroni's *post hoc* test. Measurements shown are mean ± SEM; *p < 0.05, **p < 0.01.

degradation (Svoboda and Di Cara, 2006). AU-rich elements (AREs) and cytoplasmic polyadenylation elements (CPEs) were also identified in the long 3′ UTR, but not in short 3′ UTR of *Atg8a*. CPEs enhance translation efficiency and AREs promote mRNA stability under starvation conditions (Miura et al., 2014; Yaman et al., 2002). Our results show that the CPA complex selects distal poly(A) sites during starvation, generating *Atg1* and *Atg8a* mRNAs with long 3′ UTRs, where putative stem-loop

analysis results. Genes are shown as nodes. Green node color indicates genes that are downregulated in starvation and that are CPSF5 dependent. Pink node color represents genes that are upregulated in starvation and CPSF5 dependent (B).

(C) 3′ UTR changes of transcripts involved in metabolism. RNA samples as in Figure S5G were subjected to qPCR to detect CDS and the long UTR-specific transcripts (distal 3′ UTR) of genes involved in metabolism. The relative distal 3′ UTR/CDS results for the other six genes mentioned in Figure S5G could not be measured due to qPCR primers design issues. One-way ANOVA followed by Bonferroni's *post hoc* test. Measurements shown are mean ± SEM; *p < 0.05, **p < 0.01.

(D) Illustration of the percentage of genes in various functional groups undergoing CPSF5-dependent AS among those responding to starvation.

(E) CDK8, DOA, and CPSF5 are critical for starvation-induced metabolomic changes. ATP, proteins, and triglyceride (TAG) levels were measured using whole control or mutant larvae as indicated and normalized to their weights. One-way ANOVA test was performed followed by Bonferroni's *post hoc* test. Measurements shown are mean ± SEM; *p < 0.05, **p < 0.01, ***p < 0.001.

structures, CPE, or ARE sequence elements are located—thus promoting *Atg1* and *Atg8a* mRNA stability and protein expression. These findings provide the first evidence that APA and AS are synchronized to regulate autophagy and reveal an additional layer of complexity in the regulation of starvation responses.

Posttranslational Modifications of the CDK8/DOA/CPA Complex

Previous studies suggested a relationship between 3′ UTR lengths and sensitivity to CPA factor expression (Akman et al., 2015; Baier et al., 2017). However, we did not detect any changes in CPSF6 levels using a GFP-trap line in the larval fat body during starvation. Moreover, overexpression of CPSF5 or CPSF6 failed to induce any phenotypes or autophagy, indicating that starvation does not alter the protein levels of the CFI complex (H.W.T., unpublished data). Instead, rapamycin treatment increased CPSF6 phosphorylation, revealing that posttranslational modifications regulate the activity of the CPA complex. We could not map all the phosphorylation sites on CPSF6, as the RS domain contains many arginine residues and in-gel trypsin digestion generated short peptides. Chymotrypsin digestion identified two sites, but many potential phosphorylation sites of CPSF6 were still not detected. Thus, we generated CPSF6 with mutations in all potential phosphorylation sites and a CPSF6 RS domain deletion mutant to characterize the functions of phosphorylated CPSF6.

CDK8 and DOA are ubiquitinated and degraded in a TORC1-dependent manner. Interestingly, Thr31 (T-Y motif) and Thr196 (T-F motif) of CDK8 are potential TORC1 phosphorylation sites and DOA Ser337 is a potential S6K phosphorylation site (Hsu et al., 2011). Thus, TORC1 or S6K may phosphorylate CDK8 or DOA to regulate their protein stabilities. A study showed that TORC1 activation increases the levels of many E2 and E3 components of ubiquitin ligase complexes (Chang et al., 2015). It will be interesting to investigate whether and how TORC1-dependent phosphorylation of CDK8 or DOA regulates their protein stabilities.

The CDK8/DOA/CPA Signaling Is a Conserved Regulator of Metabolism

An RNAi screen in S2R+ cells showed depletion of multiple CPA complex components increases ATP levels (Mohr et al., 2015). CDK8 is implicated in lipid metabolism, and KNS1 (DOA ortholog in yeast) in the regulation of protein homeostasis (Lee et al., 2012; Zhao et al., 2012). Here, we found the CDK8/DOA/CPA complex regulates autophagy and metabolism in both *Drosophila and* mammalian cells. As TORC1 hyperactivation and metabolic reprogramming contribute to malignancy, our study provides insight into new cancer therapeutic strategies targeting RNA metabolism downstream of the TORC1 signaling pathway.

STAR★METHODS

Detailed methods are provided in the online version of this paper and include the following:

- KEY RESOURCES TABLE
- CONTACT FOR REAGENT AND RESOURCE SHARING
- EXPERIMENTAL MODEL AND SUBJECT DETAILS
  - Experimental Animals
- METHOD DETAILS
  - Plasmid
  - Larval Starvation Procedure
  - 3′ Rapid Amplification of cDNA Ends (3′ RACE)
  - 3′ UTR Luciferase Reporter Assay
  - Cell Culture, Reagents, RNA Interference, and Transfection
  - Antibodies
  - Immunofluorescence
  - Immunoblotting
  - Quantification of mRNA Expression
  - ATP, Triglyceride, and Protein Measurements
  - Immunoprecipitation
  - *In Vitro* Kinase Assay
  - RNA Sequencing Analysis
- QUANTIFICATION AND STATISTICAL ANALYSIS
- DATA AND SOFTWARE AVAILABILITY

SUPPLEMENTAL INFORMATION

Supplemental Information includes seven figures and five tables and can be found with this article online at https://doi.org/10.1016/j.cmet.2018.02.023.

ACKNOWLEDGMENTS

We thank Harvard Catalyst and Dr. L. Liang (Harvard T.H. Chan School of Public Health) for statistical consulting, R. Kirchner (Harvard Chan Bioinformatics Core) for assistance with RNA-seq analysis, Dr. J.Y. Ji, Dr. W. Mattox, the Vienna *Drosophila* Resource Center, and Bloomington *Drosophila* Stock Center for fly stocks. We also thank G. Lee, J. Blenis, and members of the Perrimon laboratory for critical comments on the manuscript. This work was supported by the NIH (R01 AR057352 and 5P01CA120964) and the Starr Consortium (I11-0015, to N.P.). H.W.T. is supported by the Human Frontier Science Program and the Postdoctoral Research Abroad Program, sponsored by Ministry of Science and Technology, Taiwan. N.P. is a Howard Hughes Medical Institute investigator.

AUTHOR CONTRIBUTIONS

H.W.T. conceived the study and designed and performed experiments. Y.H. performed bioinformatics analyses. C.L.C. generated CRISPR mutants. B.X. performed 3′ RACE experiments. J.Z. generated transgenic flies. M.Y. and J.M.A. performed mass spectrometry experiments. L.R. provided the CLK2 antibody. H.T., L.R., and N.P. discussed results. H.T. and N.P. wrote the manuscript.

DECLARATION OF INTERESTS

The authors declare no competing interests.

Received: June 12, 2017
Revised: December 22, 2017
Accepted: February 23, 2018
Published: March 29, 2018

REFERENCES

Akman, H.B., Oyken, M., Tuncer, T., Can, T., and Erson-Bensan, A.E. (2015). 3′UTR shortening and EGF signaling: implications for breast cancer. Hum. Mol. Genet. *24*, 6910–6920.

Alamancos, G.P., Pages, A., Trincado, J.L., Bellora, N., and Eyras, E. (2015). Leveraging transcript quantification for fast computation of alternative splicing profiles. RNA *21*, 1521–1531.

Arsham, A.M., and Neufeld, T.P. (2009). A genetic screen in *Drosophila* reveals novel cytoprotective functions of the autophagy-lysosome pathway. PLoS One *4*, e6068.

Baier, R.V., Picao-Osorio, J., and Alonso, C.R. (2017). Molecular regulation of alternative polyadenylation (APA) within the *Drosophila* nervous system. J. Mol. Biol. *429*, 3290–3300.

Budovskaya, Y.V., Stephan, J.S., Deminoff, S.J., and Herman, P.K. (2005). An evolutionary proteomics approach identifies substrates of the cAMP-dependent protein kinase. Proc. Natl. Acad. Sci. USA *102*, 13933–13938.

Cardinale, S., Cisterna, B., Bonetti, P., Aringhieri, C., Biggiogera, M., and Barabino, S.M. (2007). Subnuclear localization and dynamics of the Pre-mRNA 3′ end processing factor mammalian cleavage factor I 68-kDa subunit. Mol. Biol. Cell *18*, 1282–1292.

Chabot, B., and Shkreta, L. (2016). Defective control of pre-messenger RNA splicing in human disease. J. Cell Biol. *212*, 13–27.

Chan, S., Choi, E.A., and Shi, Y. (2011). Pre-mRNA 3′-end processing complex assembly and function. Wiley Interdiscip. Rev. RNA *2*, 321–335.

Chang, J.W., Zhang, W., Yeh, H.S., de Jong, E.P., Jun, S., Kim, K.H., Bae, S.S., Beckman, K., Hwang, T.H., Kim, K.S., et al. (2015). mRNA 3′-UTR shortening is a molecular signature of mTORC1 activation. Nat. Commun. *6*, 7218.

Chang, T.H., Huang, H.Y., Hsu, J.B., Weng, S.L., Horng, J.T., and Huang, H.D. (2013a). An enhanced computational platform for investigating the roles of regulatory RNA and for identifying functional RNA motifs. BMC Bioinformatics *14* (*Suppl 2*), S4.

Chang, T.K., Shravage, B.V., Hayes, S.D., Powers, C.M., Simin, R.T., Wade Harper, J., and Baehrecke, E.H. (2013b). Uba1 functions in Atg7- and Atg3-independent autophagy. Nat. Cell Biol. *15*, 1067–1078.

Chen, G.C., Lee, J.Y., Tang, H.W., Debnath, J., Thomas, S.M., and Settleman, J. (2008). Genetic interactions between *Drosophila melanogaster* Atg1 and paxillin reveal a role for paxillin in autophagosome formation. Autophagy *4*, 37–45.

Cheong, H., Nair, U., Geng, J., and Klionsky, D.J. (2008). The Atg1 kinase complex is involved in the regulation of protein recruitment to initiate sequestering vesicle formation for nonspecific autophagy in *Saccharomyces cerevisiae*. Mol. Biol. Cell *19*, 668–681.

Dettwiler, S., Aringhieri, C., Cardinale, S., Keller, W., and Barabino, S.M. (2004). Distinct sequence motifs within the 68-kDa subunit of cleavage factor Im mediate RNA binding, protein-protein interactions, and subcellular localization. J. Biol. Chem. *279*, 35788–35797.

Dorsey, F.C., Rose, K.L., Coenen, S., Prater, S.M., Cavett, V., Cleveland, J.L., and Caldwell-Busby, J. (2009). Mapping the phosphorylation sites of Ulk1. J. Proteome Res. *8*, 5253–5263.

Feng, D., Youn, D.Y., Zhao, X., Gao, Y., Quinn, W.J., 3rd, Xiaoli, A.M., Sun, Y., Birnbaum, M.J., Pessin, J.E., and Yang, F. (2015). mTORC1 down-regulates cyclin-dependent kinase 8 (CDK8) and cyclin C (CycC). PLoS One *10*, e0126240.

Fortier, E., and Belote, J.M. (2000). Temperature-dependent gene silencing by an expressed inverted repeat in *Drosophila*. Genesis *26*, 240–244.

Gabut, M., Dejardin, J., Tazi, J., and Soret, J. (2007). The SR family proteins B52 and dASF/SF2 modulate development of the *Drosophila* visual system by regulating specific RNA targets. Mol. Cell. Biol. *27*, 3087–3097.

Ghosh, G., and Adams, J.A. (2011). Phosphorylation mechanism and structure of serine-arginine protein kinases. FEBS J. *278*, 587–597.

Guruharsha, K.G., Rual, J.F., Zhai, B., Mintseris, J., Vaidya, P., Vaidya, N., Beekman, C., Wong, C., Rhee, D.Y., Cenaj, O., et al. (2011). A protein complex network of *Drosophila melanogaster*. Cell *147*, 690–703.

Housden, B.E., and Perrimon, N. (2016). Detection of indel mutations in *Drosophila* by high-resolution melt analysis (HRMA). Cold Spring Harb. Protoc. *2016*, pdb prot090795.

Housden, B.E., Valvezan, A.J., Kelley, C., Sopko, R., Hu, Y., Roesel, C., Lin, S., Buckner, M., Tao, R., Yilmazel, B., et al. (2015). Identification of potential drug targets for tuberous sclerosis complex by synthetic screens combining CRISPR-based knockouts with RNAi. Sci. Signal. *8*, rs9.

Hsu, P.P., Kang, S.A., Rameseder, J., Zhang, Y., Ottina, K.A., Lim, D., Peterson, T.R., Choi, Y., Gray, N.S., Yaffe, M.B., et al. (2011). The mTOR-regulated phosphoproteome reveals a mechanism of mTORC1-mediated inhibition of growth factor signaling. Science *332*, 1317–1322.

Hu, G., McQuiston, T., Bernard, A., Park, Y.D., Qiu, J., Vural, A., Zhang, N., Waterman, S.R., Blewett, N.H., Myers, T.G., et al. (2015). A conserved mechanism of TOR-dependent RCK-mediated mRNA degradation regulates autophagy. Nat. Cell Biol. *17*, 930–942.

Hu, Y., Comjean, A., Roesel, C., Vinayagam, A., Flockhart, I., Zirin, J., Perkins, L., Perrimon, N., and Mohr, S.E. (2017). FlyRNAi.org-the database of the *Drosophila* RNAi screening center and transgenic RNAi project: 2017 update. Nucleic Acids Res. *45*, D672–D678.

Jiang, P., and Mizushima, N. (2014). Autophagy and human diseases. Cell Res. *24*, 69–79.

Kim, J., Kundu, M., Viollet, B., and Guan, K.L. (2011). AMPK and mTOR regulate autophagy through direct phosphorylation of Ulk1. Nat. Cell Biol. *13*, 132–141.

Kim, M., Park, H.L., Park, H.W., Ro, S.H., Nam, S.G., Reed, J.M., Guan, J.L., and Lee, J.H. (2013). *Drosophila* Fip200 is an essential regulator of autophagy that attenuates both growth and aging. Autophagy *9*, 1201–1213.

Kyburz, A., Friedlein, A., Langen, H., and Keller, W. (2006). Direct interactions between subunits of CPSF and the U2 snRNP contribute to the coupling of pre-mRNA 3′ end processing and splicing. Mol. Cell *23*, 195–205.

Lee, G., Zheng, Y., Cho, S., Jang, C., England, C., Dempsey, J.M., Yu, Y., Liu, X., He, L., Cavaliere, P.M., et al. (2017). Post-transcriptional regulation of de novo lipogenesis by mTORC1-S6K1-SRPK2 signaling. Cell *171*, 1545–1558.e18.

Lee, J., Moir, R.D., McIntosh, K.B., and Willis, I.M. (2012). TOR signaling regulates ribosome and tRNA synthesis via LAMMER/Clk and GSK-3 family kinases. Mol. Cell *45*, 836–843.

Martin, G., Gruber, A.R., Keller, W., and Zavolan, M. (2012). Genome-wide analysis of pre-mRNA 3′ end processing reveals a decisive role of human cleavage factor I in the regulation of 3′ UTR length. Cell Rep. *1*, 753–763.

Mercer, T.J., Gubas, A., and Tooze, S.A. (2018). A molecular perspective of mammalian autophagosome biogenesis. J. Biol. Chem. https://doi.org/10.1074/jbc.R117.810366.

Mihaylova, M.M., and Shaw, R.J. (2011). The AMPK signalling pathway coordinates cell growth, autophagy and metabolism. Nat. Cell Biol. *13*, 1016–1023.

Millevoi, S., Loulergue, C., Dettwiler, S., Karaa, S.Z., Keller, W., Antoniou, M., and Vagner, S. (2006). An interaction between U2AF 65 and CF I(m) links the splicing and 3′ end processing machineries. EMBO J. *25*, 4854–4864.

Miura, P., Sanfilippo, P., Shenker, S., and Lai, E.C. (2014). Alternative polyadenylation in the nervous system: to what lengths will 3′ UTR extensions take us? Bioessays *36*, 766–777.

Mohr, S.E., Hu, Y., Rudd, K., Buckner, M., Gilly, Q., Foster, B., Sierzputowska, K., Comjean, A., Ye, B., and Perrimon, N. (2015). Reagent and data resources for investigation of RNA binding protein functions in *Drosophila melanogaster* cultured cells. G3 (Bethesda) *5*, 1919–1924.

Ohsumi, Y. (2014). Historical landmarks of autophagy research. Cell Res. *24*, 9–23.

Potter, C.J., Huang, H., and Xu, T. (2001). *Drosophila* Tsc1 functions with Tsc2 to antagonize insulin signaling in regulating cell growth, cell proliferation, and organ size. Cell *105*, 357–368.

Rolland, T., Tasan, M., Charloteaux, B., Pevzner, S.J., Zhong, Q., Sahni, N., Yi, S., Lemmens, I., Fontanillo, C., Mosca, R., et al. (2014). A proteome-scale map of the human interactome network. Cell *159*, 1212–1226.

Saxton, R.A., and Sabatini, D.M. (2017). mTOR signaling in growth, metabolism, and disease. Cell *169*, 361–371.

Scott, R.C., Juhász, G., and Neufeld, T.P. (2007). Direct induction of autophagy by Atg1 inhibits cell growth and induces apoptotic cell death. Curr. Biol. *17*, 1–11.

Shi, Y., Di Giammartino, D.C., Taylor, D., Sarkeshik, A., Rice, W.J., Yates, J.R., 3rd, Frank, J., and Manley, J.L. (2009). Molecular architecture of the human pre-mRNA 3′ processing complex. Mol. Cell *33*, 365–376.

Smith, F.D., Samelson, B.K., and Scott, J.D. (2011). Discovery of cellular substrates for protein kinase A using a peptide array screening protocol. Biochem. J. *438*, 103–110.

Stephan, J.S., Yeh, Y.Y., Ramachandran, V., Deminoff, S.J., and Herman, P.K. (2009). The Tor and PKA signaling pathways independently target the Atg1/Atg13 protein kinase complex to control autophagy. Proc. Natl. Acad. Sci. USA *106*, 17049–17054.

Svoboda, P., and Di Cara, A. (2006). Hairpin RNA: a secondary structure of primary importance. Cell. Mol. Life Sci. *63*, 901–908.

Tang, H.W., Liao, H.M., Peng, W.H., Lin, H.R., Chen, C.H., and Chen, G.C. (2013). Atg9 interacts with dTRAF2/TRAF6 to regulate oxidative stress-induced JNK activation and autophagy induction. Dev. Cell *27*, 489–503.

Tang, H.W., Wang, Y.B., Wang, S.L., Wu, M.H., Lin, S.Y., and Chen, G.C. (2011). Atg1-mediated myosin II activation regulates autophagosome formation during starvation-induced autophagy. EMBO J. *30*, 636–651.

Varjosalo, M., Keskitalo, S., Van Drogen, A., Nurkkala, H., Vichalkovski, A., Aebersold, R., and Gstaiger, M. (2013). The protein interaction landscape of the human CMGC kinase group. Cell Rep. *3*, 1306–1320.

Xiang, S., Gapsys, V., Kim, H.Y., Bessonov, S., Hsiao, H.H., Möhlmann, S., Klaukien, V., Ficner, R., Becker, S., Urlaub, H., et al. (2013). Phosphorylation drives a dynamic switch in serine/arginine-rich proteins. Structure *21*, 2162–2174.

Yaman, I., Fernandez, J., Sarkar, B., Schneider, R.J., Snider, M.D., Nagy, L.E., and Hatzoglou, M. (2002). Nutritional control of mRNA stability is mediated by a conserved AU-rich element that binds the cytoplasmic shuttling protein HuR. J. Biol. Chem. *277*, 41539–41546.

Yun, B., Farkas, R., Lee, K., and Rabinow, L. (1994). The Doa locus encodes a member of a new protein kinase family and is essential for eye and embryonic development in *Drosophila melanogaster*. Genes Dev. *8*, 1160–1173.

Zhao, S., Chen, D., Geng, Q., and Wang, Z. (2013). The highly conserved LAMMER/CLK2 protein kinases prevent germ cell overproliferation in *Drosophila*. Dev. Biol. *376*, 163–170.

Zhao, X., Feng, D., Wang, Q., Abdulla, A., Xie, X.J., Zhou, J., Sun, Y., Yang, E.S., Liu, L.P., Vaitheesvaran, B., et al. (2012). Regulation of lipogenesis by cyclin-dependent kinase 8-mediated control of SREBP-1. J. Clin. Invest. *122*, 2417–2427.

STAR★METHODS

KEY RESOURCES TABLE

REAGENT or RESOURCE	SOURCE	IDENTIFIER
Antibodies		
GFP-Trap	ChromoTek	gta-20; RRID: AB_2631357
Anti-Flag agarose	Sigma	A2220; RRID: AB_10063035
Anti-HA agarose	Sigma	A2095; RRID: AB_257974
Anti-GABARAPL1/ATG8 Antibody	LSBio	LS-B12739; RRID: AB_2722618
Anti-GFP	Molecular Probes	A6455; RRID: AB_221570
Anti-phospho-Ser	Santa Cruz	sc-81514; RRID: AB_1128624
Anti-phospho-Threonine	Cell Signaling Technology	9381; RRID: AB_330301
Anti-phospho-PKA Substrate mAb	Cell Signaling Technology	9624; RRID: AB_331817
Anti-Flag	Sigma	F3165; RRID: AB_259529
Anti-HA	Covance/BioLegend	MMS-101P; RRID: AB_10064068
Anti-CDK8	Santa Cruz	sc-13155; RRID: AB_627244
Anti-LC3B	Cell Signaling Technology	2775; RRID: AB_915950
Anti-CPSF6	Santa Cruz	sc-100692; RRID: AB_1121901
Anti-ubiquitin FK2	Enzo Life Sciences	BML-PW8810-0100; RRID: AB_10541840
Anti-α-Tubulin	Sigma	T5168; RRID: AB_477579
Anti-Atg1	Kim et al., 2013	RRID: AB_2568303
Anti-CLK2	This paper	RRID: AB_2722619
Bacterial and Virus Strains		
One Shot TOP10 Chemically Competent *E. coli*	Thermo Fisher Scientific	C404003
BL21(DE3) Competent *E. coli*	NEB	C2527I
Chemicals, Peptides, and Recombinant Proteins		
Effectene transfection reagent	QIAGEN	301427
Gibco Schneider's *Drosophila* Sterile Medium	Thermo Fisher Scientific	21720024
TRIzol reagent	Invitrogen	15596-018
iScript Reverse Transcription Supermix	Bio-Rad	1708896
GoTaq Green Master mix	Promega	M7122
iQ SYBR Green Supermix	Bio-Rad	1708880
Earle's balanced salt solution (EBSS) medium	Sigma	14155063
Protease and phosphatase inhibitor cocktail	Pierce	78440
RNasin Plus RNase inhibitor	Promega	N2611
Bafilomycin A1	Sigma	B1793
Senexin A	Tocris	4875
TG003	Sigma	T5575
Rapamycin	LC Laboratories	R-5000
MG132	Calbiochem	474791
Actinomycin D	Calbiochem	114666
Chloroquine	Sigma	C6628
Glutathione Sepharose	Clontech	635607
Recombinant His-tagged human CDK8/CycC	Thermo Fisher Scientific	PV4402
Recombinant human CLK2-cat (amino acids 137–499)	Thermo Fisher Scientific	PV4201
Recombinant GST-tagged human CPSF6-N	NovoPro Bioscience	506834
Recombinant GST-tagged human CPSF6	Abnova	H00011052-P01
Recombinant GST-tagged *Drosophila* CPSF5	This paper	N/A
Recombinant GST-tagged *Drosophila* CPSF6-N	This paper	N/A

(*Continued on next page*)

Continued

REAGENT or RESOURCE	SOURCE	IDENTIFIER
Recombinant GST-tagged *Drosophila* CPSF6-C	This paper	N/A
Fetal Bovine Serum	Thermo Fisher Scientific	10437028
Glycerol standard	Sigma	G7793-5ML
Free glycerol reagent	Sigma	F6428-40ML
Triglyceride reagent	Sigma	T2449-10ML
Gateway LR Clonase II Enzyme mix	Invitrogen	11791-020
MEGAscript T7 Transcription Kit	Thermo Fisher Scientific	AMB13345
TOPO TA Cloning vector	Invitrogen	K4500-01
GST Purification Kit	Clontech	635619
BCA protein assay	Pierce	23227
pENTR/D-TOPO Cloning Kit	Invitrogen	K2400-20
Critical Commercial Assays		
Dual-Glo Luciferase Assay System	Promega	E2980
SMARTer RACE 5′/3′ Kit	Clontech	634858
CellTiter-Glo luminescent cell viability assay kit	Promega	G7573
4%–20% Mini-PROTEAN TGX Precast Protein Gels	Bio-Rad	4561096
Deposited Data		
Data files for RNA sequencing	This paper	GEO: GSE99509
Experimental Models: Cell Lines		
D. melanogaster: Cell line S2R+	Laboratory of Norbert Perrimon	N/A
D. melanogaster: TSC1 knock out S2R+	Housden et al., 2015	N/A
D. melanogaster: TSC2 knock out S2R+	Housden et al., 2015	N/A
Human: HEK293T	ATCC	CRL-11268
Human: MCF7	ATCC	HTB-22
Experimental Models: Organisms/Strains		
UAS-Atg1	BDSC	51655
UAS-mcherry-Atg8a	BDSC	37750
r4-mCherry-Atg8a Act>CD2>GAL4 UAS-GFP-nls	Arsham and Neufeld, 2009	N/A
pmCherry-Atg8a	Chang et al., 2013b	N/A
UAS-Luc-RNAi	BDSC	31603
UAS-Atg9-RNAi	VDRC	10045
UAS-Pcf11-RNAi	BDSC	32411
UAS-Cbc-RNAi	VDRC	20998, 10686
UAS-CPSF6-RNAi	BDSC	34804
UAS-CPSF6-RNAi	VDRC	107147
UAS-CPSF5-RNAi	BDSC	32883
UAS-CstF64-RNAi	VDRC	21045
UAS-Su(f)-RNAi	BDSC	43273
UAS-CstF50-RNAi	VDRC	43716
UAS-CPSF160-RNAi	BDSC	42478, 55698
UAS-Clp-RNAi	BDSC	36816
UAS-CG1109-RNAi	BDSC	55249
UAS-Fip1-RNAi	VDRC	27317
UAS-CPSF73-RNAi	BDSC	55696
UAS-CPSF73-RNAi	VDRC	39557
UAS-Sym-RNAi	BDSC	43227
UAS-CPSF100-RNAi	BDSC	50893
UAS-Pka-C1-RNAi	BDSC	31277, 58355

(*Continued on next page*)

Continued

REAGENT or RESOURCE	SOURCE	IDENTIFIER
UAS-Pka-C1-Flag	BDSC	35555
UAS-TSC1, UAS-TSC2	Potter et al., 2001	N/A
UAS-PI3K92E	BDSC	8286
UAS-Pten-RNAi	BDSC	25841, 33643
UAS-myr-AKT	BDSC	50758
UAS-TSC1-RNAi	BDSC	54034, 52931
$Rheb^{AV4}$	BDSC	9690
$UAS\text{-}TOR^{wt}$	BDSC	7012
UAS-DOA-RNAi	VDRC	19066, 102520
UAS-CycC-RNAi	BDSC	33753
UAS-CycC-RNAi	VDRC	48834
UAS-CDK8-HA	FlyORF	F001713
$Tsc2^{109}$	BDSC	4739
UAS-3XFlag-DOA	Zhao et al., 2013	N/A
$CDK8^{K185}$	Zhao et al., 2012	N/A
$CycC^{y5}$	Zhao et al., 2012	N/A
DOA^{HD}	Yun et al., 1994	N/A
DOA^{DEM}	Yun et al., 1994	N/A
UAS-CDK8-RNAi	VDRC	45371
Df(3L)AC1	BDSC	997
UAS-GFP-Atg8a	Scott et al., 2007	N/A
UAS-9G8-RNAi	VDRC	100226
UAS-GFP-9G8	Gabut et al., 2007	N/A
UAS-SRm300-RNAi	BDSC	21815, 52936
$UAS\text{-}tra2\text{-}RNAi^{G1X}$; $UAS\text{-}tra2\text{-}RNAi^{82A3}$	Fortier and Belote, 2000	N/A
UAS-Rbp1-like-RNAi	VDRC	105883
UAS-U2AF50-RNAi	BDSC	27542
UAS-InR-RNAi	BDSC	31594, 51518
UAS-PI3K92E-RNAi	BDSC	61182
UAS-Pten	BDSC	9689
UAS-Pten	Potter et al., 2001	N/A
UAS-PDK1-RNAi	BDSC	34936, 27925
UAS-AKT-RNAi	BDSC	31701
UAS-Rheb-RNAi	BDSC	33966
UAS-TOR-RNAi	BDSC	33578, 34639
UAS-HA-Atg1	This paper	N/A
$UAS\text{-}HA\text{-}Atg1^{S297A}$	This paper	N/A
$UAS\text{-}HA\text{-}CPSF6^{14A}$	This paper	N/A
$UAS\text{-}HA\text{-}CPSF6^{\Delta RS}$	This paper	N/A
$CPSF5^{H11}$	This paper	N/A
$CFSF6^{091}$	This paper	N/A
Df(3L)BSC113	BDSC	8970
Df(3L)Exel6112	BDSC	7591
Df(3L)BSC376	BDSC	24400
Df(3L)66C-G28	BDSC	1541
Df(3L)BSC815	BDSC	27576
Oligonucleotides		
Primers for 3′ RACE	This paper	See Table S5
Primers for 3′ UTR luciferase reporter assay	This paper	See Table S5

(*Continued on next page*)

Continued

REAGENT or RESOURCE	SOURCE	IDENTIFIER
Primers for mRNA expression	This paper	See Table S5
Primers for RNA- Immunoprecipitation	This paper	See Table S5
CPSF6 shRNA #1	Sigma, clone ID: TRCN0000237833	GTTGTAACTCCATGCAATAAA
CPSF6 shRNA #2	Sigma, clone ID: TRCN0000244314	GGTGATTATGGGAGTGCTATT
Recombinant DNA		
pAWG-Atg1-PB	This paper	N/A
pAWG-CPSF5	This paper	N/A
pAWG-CPSF6	This paper	N/A
pAWG-CstF64	This paper	N/A
pAWG-CPSF160	This paper	N/A
pAWG-Cbc	This paper	N/A
pAWG-Pcf11	This paper	N/A
pAWM-GFP	This paper	N/A
pAWG-CPSF6ΔRS	This paper	N/A
pcDNA3.1-Flag-CDK8	This paper	N/A
pWALIUM10-moe-HA-DOA	This paper	N/A
pAWG-Atg1-PB-S279A	This paper	N/A
pAWG-CPSF6^{14A}	This paper	N/A
pTWH-Atg1	This paper	N/A
pTWH-Atg1^{S297A}	This paper	N/A
pTWH-CPSF6^{14A}	This paper	N/A
pTWH-CPSF6$^{\Delta RS}$	This paper	N/A
pGEX-2T-CPSF5	This paper	N/A
pGEX-2T-CPSF6N	This paper	N/A
pGEX-2T-CPSF6C	This paper	N/A
pReceiver-M29-N-eGFP-CPSF6	GeneCopoeia	EX-Mm18988-M29
UAS-Flag-Fip200	Kim et al., 2013	N/A
Software and Algorithms		
ZEN 2 lite	Zeiss	N/A
COMPLEAT	Hu et al., 2017	N/A
RegRNA	Chang et al., 2013a	N/A
Prism	GraphPad Software	N/A
ImageJ	NIH	N/A
Other		
Label-free quantitative Mass Spectrometry Data	This paper	N/A
Zeiss LSM780 microscope	Zeiss	N/A
CFX96 Real-Time System	Bio-Rad	N/A

CONTACT FOR REAGENT AND RESOURCE SHARING

Further information and requests for resources and reagents should be directed to and will be fulfilled by the Lead Contact, Norbert Perrimon (perrimon@receptor.med.harvard.edu).

EXPERIMENTAL MODEL AND SUBJECT DETAILS

Experimental Animals

Species: Drosophila melanogaster

Flies were raised in a humidified incubator at 25°C with 12/12 hr dark/light cycles (lights on at 7 am) on standard lab food containing per liter: 15 g yeast, 8.6 g soy flour, 63 g cornmeal, 5g agar, 5g malt, 74 mL corn syrup. Mixed sex second instar larvae were used in experiments. The following *Drosophila* strains from previous studies, Bloomington Drosophila stock center (BDSC), or Vienna

Drosophila Resource center (VDRC), were used: *UAS-Atg1* (BDSC51655), *UAS-mcherry-Atg8a* (BDSC37750), *r4-mCherry-Atg8a Act>CD2>GAL4 UAS-GFP-nls* (Arsham and Neufeld, 2009), *pmCherry-Atg8a* (Chang et al., 2013b), *UAS-Luc-RNAi* (BDSC31603), *UAS-Atg9-RNAi* (VDRC10045), *UAS-Pcf11-RNAi* (BDSC32411), *UAS-Cbc-RNAi* (VDRC20998 and VDRC10686), *UAS-CPSF6-RNAi* (BDSC34804 and VDRC107147), *UAS-CPSF5-RNAi* (BDSC32883), *UAS-CstF64-RNAi* (VDRC21045), *UAS-Su(f)-RNAi* (BDSC43273), *UAS-CstF50-RNAi* (VDRC43716), *UAS-CPSF160-RNAi* (BDSC42478 and BDSC55698), *UAS-Clp-RNAi* (BDSC36816), *UAS-CG1109-RNAi* (BDSC55249), *UAS-Fip1-RNAi* (VDRC27317), *UAS-CPSF73-RNAi* (BDSC55696 and VDRC39557), *UAS-Sym-RNAi* (BDSC43227), *UAS-CPSF100-RNAi* (BDSC50893), *UAS-Pka-C1-RNAi* (BDSC31277 and BDSC58355), *UAS-Pka-C1-Flag* (BDSC35555), *UAS-TSC1*, *UAS-TSC2* (Potter et al., 2001), *UAS-PI3K92E* (BDSC8286), *UAS-Pten-RNAi* (BDSC25841 and BDSC33643), *UAS-myr-AKT* (BDSC50758), *UAS-TSC1-RNAi* (BDSC54034 and BDSC52931), $Rheb^{AV4}$ (BDSC9690), $UAS\text{-}TOR^{wt}$ (BDSC7012), *UAS-DOA-RNAi* (VDRC19066 and VDRC102520), *UAS-CycC-RNAi* (BDSC33753 and VDRC48834), *UAS-CDK8-HA* (FlyORF F001713), $Tsc2^{109}$ (BDSC4739), *UAS-3XFlag-DOA* (Zhao et al., 2013), $CDK8^{K185}$ (Zhao et al., 2012), $CycC^{y5}$ (Zhao et al., 2012), DOA^{HD} and DOA^{DEM} (Yun et al., 1994), *UAS-CDK8-RNAi* (VDRC45371), *Df(3L)AC1* (BDSC997), *UAS-GFP-Atg8a* (Scott et al., 2007), *UAS-9G8-RNAi* (VDRC100226), *UAS-GFP-9G8* (Gabut et al., 2007), *UAS-SRm300-RNAi* (BDSC21815 and BDSC52936), $UAS\text{-}tra2\text{-}RNAi^{G1X}$; $UAS\text{-}tra2\text{-}RNAi^{82A3}$ (a gift of Dr. W. Mattox.) (Fortier and Belote, 2000), *UAS-Rbp1-like-RNAi* (VDRC105883), *UAS-U2AF50-RNAi* (BDSC27542), *UAS-InR-RNAi* (BDSC31594 and BDSC51518), *UAS-PI3K92E-RNAi* (BDSC61182), *UAS-Pten* (BDSC9689 and Potter et al., 2001), *UAS-PDK1-RNAi* (BDSC34936 and BDSC27925), *UAS-AKT-RNAi* (BDSC31701), *UAS-Rheb-RNAi* (BDSC33966), and *UAS-TOR-RNAi* (BDSC33578 and BDSC34639). The *UAS-HA-Atg1*, $UAS\text{-}HA\text{-}Atg1^{S297A}$, $UAS\text{-}HA\text{-}CPSF6^{14A}$, and $UAS\text{-}HA\text{-}CPSF6^{\Delta RS}$ transgenes were generated from plasmids described below and cloned into the *Drosophila* Gateway vector pTWH. Mutant alleles for *CPSF5* and *CPSF6* were generated using CRISPR technology. Two independent guide RNAs (gRNAs) per gene were designed using the gRNA design tool: http://www.flyrnai.org/crispr/index.html. Oligonucleotides were annealed and cloned into the pl100 vector. Vectors were injected into *w;nos-cas9/CyO* embryos. Wings of single flies were clipped to isolate DNA and high-resolution melt analysis (HRMA) analysis was used to detect indel mutations (Housden and Perrimon, 2016). Candidate flies were crossed with *y w; TM3/TM6b* to establish stocks. The $CPSF5^{H11}$ allele was obtained using the gRNA sequence GTCTCAAACAAATCGGGCTC and found to carry to a 13 bp deletion leading to a frame shift and a potential 36 aa peptide (Table S4). The $CFSF6^{091}$ allele was obtained using the gRNA sequence GTACAGATCCAAGACCACGT and found to correspond to an indel with a premature stop codon and a potential truncated protein of 31a.a (Table S4). $CPSF5^{H11}$ allele is homozygous lethal and failed to complement deficiencies uncovering *CPSF5* (BDSC8970 and BDSC997). $CFSF6^{091}$ is homozygous lethal and failed to complement deficiencies uncovering *CPSF6* (BDSC7591, BDSC24400, BDSC1541, and BDSC27576).

Cell Lines

Drosophila S2R+ cells (sex: male) were cultured in Schneider's medium supplemented with 10% fetal bovine serum (FBS) at 25°C. HEK293T (sex: female) and MCF7 (sex: female) cells were cultured at 37°C in DMEM (Invitrogen, 10-017-CV) medium supplemented with 10% FBS.

METHOD DETAILS

Plasmid

The full-length cDNAs of *Atg1* (LD18893), *CPSF5* (SD03330), *CPSF6* (LD25239), *CstF64* (RE27227), *CPSF160* (LD38533), *Cbc* (LD15072) and *Pcf11* (MIP05908), were cloned into the *Drosophila* Gateway vector pAWG. GFP was cloned into pAWM as a control. *GFP- CPSF6*$^{\Delta RS}$ (amino acids 1-400) which contains the RRM domain was created by PCR amplification and verified by DNA sequencing. Flag-CDK8 and HA-DOA were constructed following PCR from cDNA clones (RE13344 and RE04477) and cloned into pcDNA3.1-Flag and pWALIUM10-moe, respectively. Using PCR mutagenesis, we generated CDK8-KD (kinase-dead) and DOA-KD mutants by replacing the conserved ATP-binding Lysine 52 and Lysine 193 in the kinase domain with Alanine, respectively. The *Atg1-PB-S279A* mutant was generated by replacing Serine 297 with Alanine. *CPSF6*^{14A} was generated by custom gene synthesis (IDT) and replacing Serines 459, 468, 525, 527, 531, 541, 543, 549, 571, 573, 588, 596, 622, and Threonine 404 with Alanines and cloned into *Drosophila* Gateway vector pAWG. For the generation of the GST fusion protein, DNA sequences corresponding to amino acids 1-240 and 221-652 of CPSF6 and full length of *CPSF5* were PCR-amplified and subcloned into the pGEX-2T vector. GFP-human CPSF6 was obtained from GeneCopoeia (EX-Mm18988-M29). *UAS-Flag-Fip200* was a gift of Dr. Jun Hee Lee (Kim et al., 2013).

Larval Starvation Procedure

Second larvae were collected 72-96 hr after egg laying and then cultured in fresh fly media supplemented with yeast paste (Fed), or in vials containing 20% sucrose (Starved) for 4 hr or 16 hr.

3′ Rapid Amplification of cDNA Ends (3′ RACE)

Total RNA was extracted from larval fat body using TRIzol reagent (Invitrogen, 15596-018). 4 μg of total RNA was used for cDNA synthesis and 3′ RACE by using SMARTer RACE 5′/3′ Kit (Clontech, 634858). Gene-specific forward primers and a universal reverse primer were used for the first-round and nested PCR amplification as indicated. The PCR products were cloned using TOPO TA Cloning vector (Invitrogen, K4500-01) and sequenced. Gene specific primers are listed in Table S5.

3′ UTR Luciferase Reporter Assay

The firefly luciferase reporter plasmids containing long or short 3′ UTRs of *Atg1* and *Atg8a* were constructed using the primers listed in Table S5. Experiments were performed in 96-well plates excluding the outer wells. Cells were transfected with firefly luciferase reporter plasmids and Renilla luciferase reporter plasmid for transfection control. After 72 hr, luciferase activities were measured using DualGlo (Promega, E2980).

Cell Culture, Reagents, RNA Interference, and Transfection

Drosophila wild-type, TSC1KO and TSC2KO S2R+ cells (Housden et al., 2015) were cultured in Schneider's medium supplemented with 10% fetal bovine serum (FBS) at 25°C. For Rapamycin (LC Laboratories, R-5000), MG132 (Calbiochem, 474791), or Actinomycin D (Calbiochem, 114666) treatment, S2R+ cells were treated with 20 nM Rapamycin or 20 μM MG132 for 24 hr, or 10 μg/mL Actinomycin D for the indicated time points.

For RNAi experiments, PCR templates for dsRNA against *PKA* (DRSC03399 and DRSC31381) *CDK8* (DRSC28684 and DRSC41558) and *DOA* (DRSC16650 and DRSC40713) were prepared using the MEGAscript T7 Transcription Kit (Invitrogen, AMB13345). DsRNA against the bacterial β-galactosidase gene (lacZ) was used as a control. S2R+ cells were dispensed into assay plates containing dsRNAs at a standard concentration for the 'bathing' method (https://fgr.hms.harvard.edu/drsc-cell-rnai).

HEK293T and MCF7 cells were cultured at 37°C in DMEM (Invitrogen, 10-017-CV) medium supplemented with 10% FBS (complete medium). For nutrient starvation, cells were starved for 2 hr in serum-free Earle's balanced salt solution (EBSS) medium (Sigma, 14155063) plus 100 nM Bafilomycin A1 (Sigma, B1793), 50 μM Senexin A (Tocris, 4875), or 50 μM TG003 (Sigma, T5575) where indicated. The production and infection of lentivirus carrying *CPSF6* shRNA clones were performed as described previously (Tang et al., 2011, 2013). The target sequences of these clones are *CPSF6* shRNA #1: (Clone ID: TRCN0000237833) 5′ GTTGTAACTCC ATGCAATAAA 3′ and *CPSF6* shRNA #2: (Clone ID: TRCN0000244314) 5′ GGTGATTATGGGAGTGCTATT 3′. Luciferase shRNA was used as a control.

Antibodies

Antibodies used for the study were: anti-Atg8 (LSBio, LS-B4021), anti-GFP (Molecular Probes, A6455), anti-phospho-Ser (Santa Cruz, sc-81514), anti-phospho-Threnonine (Cell Signaling, 9381), anti-Phospho-PKA substrate (Cell Signaling, 9624), anti-Flag (Sigma, F3165), anti-HA (Covance/BioLegend, MMS-101P), anti-CDK8 (Santa Cruz, sc-13155), anti-LC3B (Cell Signaling, 2775), anti-human CPSF6 (Santa Cruz, sc-100692), anti-ubiquitin FK2 (Enzo life Science, BML-PW8810-0100), and anti-Tubulin (Sigma, T5168). Anti-Atg1 was a gift of Dr. Jun Hee Lee (Kim et al., 2013). Anti-CLK2 was produced by cloning via PCR a 1.3 kb fragment encoding the catalytic domain of human CLK2 from a full-length cDNA in frame into the BamHI site in the pMAL-C2 vector (New England Biolabs). It was expressed in *E. coli* as a fusion protein with the Maltose Binding Protein. Following purification on an amylose column, the recombinant protein was injected into two rats for antibody production.

Immunofluorescence

Eye imaginal discs from wandering third instar larvae were dissected, fixed with 4% paraformaldehyde, and mounted. GFP-marked flip clones in the larval fat body were generated through heat shock-independent induction as previously described (Tang et al., 2013). For lipid droplet staining, larvae were dissected in PBS and fixed in 4% paraformaldehyde for 30 min at room temperature. Larval fat body was then washed with PBS, incubated for 15 min in 2 μg/mL Nile red/PBS, and then mounted. S2R+ cells were fixed with 4% paraformaldehyde and MCF7 cells were fixed with ice-cold 100% methanol. Cells were then permeabilized with 0.1% triton and processed for immunostaining. DAPI (1 μg/mL) was used to stain nuclei. Samples were examined using *a* confocal laser scanning microscope (LSM780; Carl Zeiss) equipped with a 63x Plan-Apochromat (NA1.4) objective lens.

Immunoblotting

Larvae were collected 72-96 hr after egg laying, cultured in fresh fly media supplemented with yeast paste (Fed) and 10 mg/mL CQ (Fed+CQ), or in vials containing 20% sucrose (Starved) and 10 mg/mL CQ (Starved+CQ) for 4 hr or 16 hr prior to dissection. After dissection, the samples were then boiled in SDS sample buffer, run on a 4%–20% polyacrylamide gel (Bio-Rad, 4561096), and transferred to an Immobilon-P polyvinylidene fluoride (PVDF) *membrane* (Millipore). The membrane was blocked by 5% BAS in TBST (TBS with 0.1% Tween-20) in room temperature for 1 hr and then probed with primary antibody in 1X TBST with 5% BSA overnight, followed by HRP-conjugated secondary antibody, and signal was detected by enhanced chemiluminescence (ECL; Amersham, RPN2209; Pierce, 34095).

Quantification of mRNA Expression

Total RNA was extracted from larval fat body using TRIzol reagent (Invitrogen 15596-018). We synthesized first strand cDNA with 1 μg of total RNA using iScript Reverse Transcription Supermix (BIO-RAD, 1708896) and then performed RT-PCR using GoTaq Green Master mix (Promega, M7122) or quantitative PCR with CFX96 Real-Time System (BIO-RAD) using iQ SYBR Green Supermix (BIO-RAD, 1708880). All expression values were normalized to RpL32 (also known as rp49). All assays were performed in triplicate. The primer sequences used for PCR are listed in Table S5.

ATP, Triglyceride, and Protein Measurements

MCF7 cells or six larvae from each group were homogenized in PBS supplemented with 0.1% Triton X-100 and Proteinase inhibitor cocktail (Pierce, 78440), heated at 70C for 5 min, and the supernatant collected after centrifugation at 14,000 rpm for 10 min. Supernatants were then subjected to TAG and Protein measurement using a Serum Triglyceride Determination kit (Sigma, T2449) and a BCA protein assay (Pierce, 23227) following the manufacturer's protocol. For ATP assay, larvae or cells were lysed in CellTiter-Glo buffers and lysates were subjected to ATP measurement using the CellTiter-Glo luminescent cell viability assay kit (Promega, G7573). For the *Drosophila* studies, ATP, triglyceride, and protein values were normalized to larval weight.

Immunoprecipitation

DNA was transfected into S2R+ or HEK293T cells in a 10 cm plate with Effectene transfection reagent (Qiagen, 301427) following the manufacturer's protocol. After 3 days of incubation, cells were lysed with lysis buffer (Pierce 89901 and 87788) with 2X protease and phosphatase inhibitor cocktail (Pierce, 78440) or RNasin Plus RNase inhibitor (Promega, N2611). Lysate was incubated with Chromotek-GFP-Trap (Bulldog Biotechnology, gta-20), anti-HA agarose (Sigma, A2095) or anti-Flag agarose (Sigma, A2220) for 1-2 hr at 4°C to precipitate the protein complexes. Beads were washed 3-4 times with 1 mL lysis buffer. Phosphorylated protein-RNA complexes were subjected to label-free quantitative mass spectrometry with in-gel digestion using Chymotrypsin or detected by western blotting or qPCR. The primer sequences used for RNA- Immunoprecipitation are listed in Table S5.

In Vitro Kinase Assay

Recombinant human proteins used for the study were: His-tagged CDK8/CycC (Thermo Fisher Scientific, PV4402), CLK2-cat (amino acids 137-499) (Thermo Fisher Scientific, PV4201), GST-tagged CPSF6-N (NovoPro Bioscience, 506834), and GST-tagged CPSF6 (Abnova, H00011052-P01). To generate recombinant *Drosophila* proteins, various segments of *CPSF6* cDNA were cloned into pGEX-2T and recombinant CPSF6 proteins were purified from bacteria and eluted from Glutathione Sepharose (Clontech, 635607) as suggested by the manufacturer. S2R+ cells expressing HA-DOA, GFP-ATG1-PB, or ATG1-PB-S297A or HEK 293T cells expressing FLAG-CDK8 were lysed in lysis buffer (Pierce, 87788) with protease and phosphatase inhibitor cocktail (Pierce, 78440) and the lysates were immunoprecipitated. Kinase reactions were carried out in a kinase reaction buffer containing the immune complex, recombinant proteins, and [r-32P] ATP as described previously (Tang et al., 2011).

RNA Sequencing Analysis

Total RNA was extracted from larval fat body using TRIzol reagent (Invitrogen, 15596-018). After assessing RNA quality with an Agilent Bioanalyzer, libraries constructed with an Illumina TruSeq Stranded Total RNA Library Prep Kit with Ribo-Zero Gold were sequenced using an Illumina HiSeq 4000 at the Columbia Genome Center (http://systemsbiology.columbia.edu/genome-center). We multiplexed samples in each lane, which yields a targeted number of paired-end 100-bp reads for each sample. The raw data files of sequencing reads were processed at Harvard Chan Bioinformatics Core with the bcbio-nextgen pipeline, version 1.0.0a0-4708de9 (http://bcbio-nextgen.readthedocs.io/). For quality control purposes, the reads were aligned to *Drosophila* genome version BDGP6 with STAR version 2.5.3 (https://github.com/alexdobin/STAR) and the alignments were evaluated based on the mappability to transcripts and the complexity of the transcriptome as well as the quality among other custom metrics. The expression of transcripts was quantified using Sailfish 0.10.1 (https://github.com/kingsfordgroup/sailfish) taking 30 bootstrap samples for each sample. Gene level expression was calculated by collapsing the transcript-level quantification with tximport (https://github.com/mikelove/tximport). Differentially expressed genes were analyzed with DESeq2 version 1.14.1 (https://bioconductor.statistik.tu-dortmund.de/packages/3.4/bioc/html/DESeq2.html) while differentially expressed transcripts were analyzed with sleuth version 0.28.1 (https://github.com/pachterlab/sleuth), leveraging the bootstrap samples to account for technical variability assigning reads to individual transcripts. The final hits of differentially expressed genes as well as transcripts were selected based on both fold changes comparing to the control larval fat body as well as adjusted p value calculated by DESeq or sleuth. TPM values were used to calculate the fold changes. Hits were selected if 2 or more-fold changes were consistently observed among the replicates and the adjusted p value is less than 0.05. The genes or transcripts that do not meet the 2-fold change cutoff with any of the replicates but with adjusted p value of 0.01 or less are included as low confidence hits in Table S2 but were not selected for enrichment analysis. Gene set enrichment analysis was performed using an in-house java program based on hypergeometric distribution. For *Drosophila* genes, gene sets were assembled using gene ontology annotation, pathway annotation from GLAD, and protein complex annotation from COMPLEAT (Hu et al., 2017). Human pathway annotation of Reactome and KEGG were mapped to *Drosophila* gene sets using DIOPT (Hu et al., 2017). The heatmap of the selected gene sets were obtained using TM4 software suite (http://mev.tm4.org/). We selected the starvation responsive genes that are CPSF5 dependent and also part of selected gene sets (energy metabolism, ribosome, lipid metabolism, glycolysis, and autophagy) and built a protein-protein interaction network based on integrated network from BioGRID, InAct, MINT, DIP, DroID,DPiM and FlyBase. Solid edges are protein-protein interactions identified in *Drosophila* while the dotted lines are for interologs, protein-protein interactions derived from data in other species. Network visualization was done using Cytoscape vs 3.1.0 (http://www.cytoscape.org/) (https://github.com/cytoscape).

QUANTIFICATION AND STATISTICAL ANALYSIS

Statistical analyses were performed in GraphPad Prism. Student's t test was used for pairwise comparisons, whereas multiple comparisons were analyzed with one-way analysis of variance (ANOVA) and Bonferroni's post hoc test. No particular methods were used to determine whether the data met assumptions of the statistical approach. Statistical parameters can be found in the figure legends.

DATA AND SOFTWARE AVAILABILITY

The accession number for the RNA-seq data reported in this paper is GEO: GSE99509.

Cell Metabolism, Volume *27*

Supplemental Information

The TORC1-Regulated CPA Complex Rewires an RNA Processing Network to Drive Autophagy and Metabolic Reprogramming

Hong-Wen Tang, Yanhui Hu, Chiao-Lin Chen, Baolong Xia, Jonathan Zirin, Min Yuan, John M. Asara, Leonard Rabinow, and Norbert Perrimon

Figure S1. Function of the CPA complex and CPA-interacting splicing factors in autophagy. Related to Figure 2.

(A-B) Identification of polyadenylation sites in 3'UTR of *Atg1* and *Atg8a* by 3'RACE. Position of the polyA sites are indicated by an arrow in the 3'UTR sequences of *Atg1* (A) and *Atg8a* (B). (C) Expression of $Pcf11^{RNAi}$ or Cbc^{RNAi} in the larval fat body induced 3'UTR extension of *Atg1* and *Atg8a* under fed conditions. The ratio between amplicons (Distal 3'UTR/CDS) represents APA isoform changes. (D) Relative mRNA expression of *Atg1* and *Atg8a* transcripts. Compared with control under fed condition (starvation 0 hr), *Atg1* and *Atg8a* mRNAs increased in fat bodies from starved control larva (starvation 4 and 16 hrs), but not from $CPSF6^{RNAi}$, Clp^{RNAi}, or $CstF64^{RNAi}$-expressing larva under starvation for 16 hrs. (E) Long 3'UTRs of *Atg1* and *Atg8a* enhanced protein expression. *Firefly Luciferase* reporters with the indicated 3'UTRs were transfected into S2R+ cells. After 48 hrs, cells were treated with Rapamycin (20 nM) for 24 hrs, followed by measuring Luciferase activity (Student's T-test was performed; data represent as mean ± SEM; *P<0.05, **P<0.01). (F-G) The CPA complex regulates ATG1 and ATG8a protein levels in the larval fat body. Protein extracts from fat bodies of fed or starved larvae with or without Chloroquine (CQ) treatment were subjected to western blot analysis using antibodies as indicated (F). (G) For quantification, the protein levels of ATG1 and ATG8a (with Chloroquine treatment) in each genotype were measured with ImageJ and normalized to the Tubulin levels. Data are expressed as a fold change compared with the wild-type controls under fed condition. One-Way ANOVA test was performed followed by Bonferroni's post hoc test. Measurements shown are mean ± SEM of triplicates; *P<0.05, **P<0.01, ***P<0.001. (H-I) The CPA complex mediates starvation-induced AS of *Atg1* through 9G8 and U2AF50. RNA extracted from larval fat bodies were subjected to RT-PCR analysis to detect the two AS isoforms, *RA* and *RB,* and the long-UTR specific transcripts (Distal 3'UTR) of *Atg1*. Depletion of *Pcf11*, *Cbc,* or *9G8*, induced alternative splicing of *Atg1* isoforms and extended *Atg1* 3'UTR length under fed conditions (H). *Atg1* isoform conversion and

3'UTR length change induced by *Cbc*^{RNAi} was suppressed by co-expressing either *9G8* or *U2AF50*^{RNAi} (I). (J-P) 9G8 and U2AF50 regulate autophagy. Expression of *9G8*^{RNAi} (J) induces mCherry-ATG8a puncta formation in the fed condition. Conversely, expression of *GFP-9G8* (K) or *U2AF50*^{RNAi} (O), but not *SRm300*^{RNAi} (L), *Tra2*^{RNAi} (M), or *Rbp1-like*^{RNAi} (N), repress mChrry-ATG8a puncta formation induced by starvation. (P) Quantification of the relative number of mCherry-ATG8a dots per cell (Student's T-test was performed to identify significant differences between mCherry dot numbers in clones and dot numbers in control cells outside of the clones; data represent the mean± SEM of 3 fat-body samples imaged per genotype; **P<0.01, ***P<0.001). Scale bar, 20 μm. (Q-S) Atg1^{S297A} mutation induced higher autophagic level than wild-type Atg1. More mCherry-ATG8a puncta were induced in clonal expression of *Atg1*^{S297A}, compared to wild-type *Atg1* (M). (N) Quantification of the relative number of mCherry-ATG8a dots per cell (One-Way ANOVA test was performed followed by Bonferroni's post hoc test; data are represented as mean ± SEM; *P<0.05). Protein extracts from the *Atg1-RB*- or *Atg1-RB*^{S297A}-expressing fat bodies of fed larvae with Chloroquine (CQ) treatment were subjected to western blot analysis using antibodies as indicated (S).

Figure S2. The PI3K/AKT/TORC1 pathway regulates APA and AS of *Atg1* and *Atg8a* as well as CPSF6 phosphorylation. Related to Figure 3.

(A-B) Inhibition of the TORC1 signaling induced AS and APA of *Atg1* and *Atg8a*. Larval fat bodies under fed or starved conditions were dissected and subjected to qPCR or RT-PCR analysis using pairs of primers (Figure 2A). *InR*^{RNAi}*, PI3K92E, Pten, PDK1*^{RNAi}*, AKT*^{RNAi}*, Rheb*^{RNAi}*, or TOR*^{RNAi}, induced 3'UTR extension of *Atg1* and *Atg8a* (A) as well as *Atg1* isoforms conversion (B). One-Way ANOVA test was performed followed by Bonferroni's post hoc test. Data are represented as mean ± SEM; *P<0.05, **P<0.01. (C-D) TORC1 activation suppresses CPSF6 phosphorylation. Wild-type, TSC1-KO, or TSC2-KO S2R+ cells transfected with *GFP, GFP-CPSF6, GFP-CPSF160, or GFP-CstF64,* were treated with or without Rapamycin (20 nM) for 24 hrs and then subjected to immunoprecipitation with anti-GFP nanobody. Immunoprecipitated proteins were analyzed by

immunoblotting. The phosphorylation signal of CstF64 was detected, but Rapamycin treatment did not affect it (C). Moreover, the phosphorylation of CPSF6 is repressed in *TSC1-KO* or *TSC2-KO* cells (D).

Figure S3. The CDK8/DOA complex is degraded by TORC1-dependent ubiquitination and interacts with RS domain of CPSF6. Related to Figure 4.

(A) *CDK8/CycC* genetically interacts with *DOA*. Clonal expression of *CDK8* or *DOA* induced mCherry-ATG8a puncta formation in the larval fat body under fed conditions. Depletion of *DOA* or *CycC* can inhibit the CDK8- or DOA-induced effects respectively. Fat body cells are stained with DAPI. (B) Quantification of the relative number of mCherry-ATG8a dots per cell. (One-Way ANOVA test was performed followed by Bonferroni's post hoc test; data are represented as mean ± SEM; ***P<0.001) (C) CDK8 physically interacts with DOA. S2R+ cells, transfected with *Flag-tagged CDK8* and *HA-tagged DOA*. After 48 hrs, cells were treated with Rapamycin (20 nM) for 24 hrs and lysates immunoprecipitated with anti-HA agarose. Immunoprecipitated proteins and total cell lysates (TCL) were analyzed by immunoblotting (IB) with antibodies as indicated. (D) Effects of Rapamycin treatment on the protein levels of CDK8 and DOA. S2R+ cells transfected with *Flag-tagged CDK8* or *HA-tagged DOA* were treated with or without Rapamycin (20 nM) for 24 hrs. Total cell lysates were analyzed by immunoblotting (IB) with antibodies as indicated. (E) TORC1 activity is required for ubiquitination of CDK8 and DOA. S2R+ cells transfected with *Flag-tagged CDK8* or *HA-tagged DOA* were treated with or without Rapamycin (20 nM) in the presence or absence of MG132 (20 μM) for 24hrs and then subjected to immunoprecipitation (IP) with anti-Flag or anti-HA antibodies. Immunoprecipitated proteins and total cell lysates (TCL) were analyzed by immunoblotting (IB). (F) Schematic representation of the domain structures of CPSF6 and RS domain deletion mutants ($CPSF6^{\Delta RS}$). (G-H) CDK8 and DOA physically interact with the RS domain of CPSF6. S2R+ cells, transfected with *GFP, GFP-tagged CPSF6,* or *GFP-tagged*

RS deletion mutant of CPSF6 (CPSF6$^{\Delta RS}$), together with *Flag-tagged CDK8* (L) or *HA-tagged DOA* (M). After 48 hrs, cells were treated with or without Rapamycin (20 nM) for 24 hrs and lysates immunoprecipitated with anti-GFP nanobody. Immunoprecipitated proteins and total cell lysates (TCL) were analyzed by immunoblotting (IB) with antibodies as indicated.

Figure S4. Physiological functions of CPSF6 phosphorylation. Related to Figure 5.

(A) Shown is the amino acid sequence of CPSF6 C-terminal region containing RS domain (401aa - 652aa). The CDK8 consensus phosphorylation sites are indicated by blue boxes and the DOA consensus phosphorylation sites are indicated by red boxes. Purified recombinant CPSF6-C phosphorylated by CDK8 or DOA as described in Figure 2N-O was digested with Chymotrypsin and then subjected to mass spectrometry analysis. The inverted triangles indicate Ser-588 and Ser596 of CPSF6, identified as DOA and CDK8 phosphorylation sites respectively. (B) Quantification of CPSF6 phosphorylation on S588 and S596 residues in vivo. S2R+ cells were transfected with *GFP-CPSF6* with or without Rapamycin (20 nM) and then subjected to immunoprecipitations. The immunoprecipitated CPSF6 proteins were subjected to label-free quantitative mass spectrometry. % occupancy was calculated by dividing the total ion current (TIC) for the phosphorylated peptide by the sum of TIC for both the phosphorylated and unphosphorylated cognate peptide. (C) CDK8 and DOA are required for the Rapamycin-induced phosphorylation of the CPSF6 RS domain. S2R+ cells were treated with dsRNA against LacZ, CDK8, or DOA. After 48 hrs, cells were transfected with *GFP, GFP-CPSF6, GFP-CPSF6^{14A}*, or *GFP-CPSF6$^{\Delta RS}$*, with or without Rapamycin (20 nM) and then subjected to immunoprecipitation. Immunoprecipitated proteins were analyzed by immunoblotting (IB) with antibodies as indicated. (D) TORC1 activity regulates CPSF6 localization. Wild-type, TSC1-KO, or TSC2-KO S2R+ cells, transfected with *GFP* or *GFP-CPSF6,* were treated with or without Rapamycin (20 nM) for 24 hrs and then subjected to immunofluorescence. GFP-CPSF6 was localized in the nuclei of control

cells (wild-type), whereas it redistributed to the cytoplasm in TSC1-KO or TSC2-KO cells. The redistribution of CPSF6 was blocked in TSC1-KO or TSC2-KO cells treated with Rapamycin. Scale bar, 10 mm. (E) TORC1 activity negatively regulates the association between CPSF6 and *Atg* transcripts. Cells were treated as in (D) and then subjected to RNA-immunoprecipitation. Immunoprecipitated RNAs and RNAs of total cell lysates were analyzed by qPCR with pairs of primers (Figure 2A) that detect total transcript (CDS) of *Atg1* or *Atg8a*. Plotted fold change values (ratios of RNA IP/input normalized to GFP control) are the mean ± SEM of triplicates. One-Way ANOVA test was performed followed by Bonferroni's post hoc test; *P<0.05, **P<0.01. (F-H) Phosphorylation of CPSF6 regulates APA and AS of *Atg1* and *Atg8a* transcripts as well as ATG1 and ATG8a protein levels in the larval fat body. Compared with control (starvation 16hrs), expression of CPSF6 with mutations of all fourteen phosphorylatable sites to Alanine ($CPSF6^{14A}$) or CPSF6 carrying a deletion of the RS domain ($CPSF6^{\Delta RS}$) in larval fat body decreased the 3'UTR length of *Atg1* and *Atg8a* transcripts (F), inhibited alternative splicing of *Atg1* isoforms (G), and reduced ATG1 and ATG8a protein levels (H). One-Way ANOVA test was performed followed by Bonferroni's post hoc test; data are represented as mean ± SEM; **P<0.01, ***P<0.001). (I) ATG1 and ATG8a protein were decreased in the larval fat body of CPSF5, CDK8, or DOA mutants. Western blot probed using anti-ATG1, anti-ATG8a, and anti-Tubulin antibodies.

Figure S5. Gene set and protein complex enrichment analyses focusing on autophagy and metabolism. Related to Figure 6.

(A-E) Representative genes involved in energy metabolism (A), ribosome (B), glycolysis (C), autophagy (D), and lipid digestion (E). These biological processes were significantly affected in fat bodies of starved larvae, and the changes could be reversed in fat bodies of starved *CPSF5* mutant larvae. The heat map signals represent the log2 ratio that is normalized to the mean of each gene. Yellow signal denotes higher expression and blue signal denotes lower expression

relative to the mean expression level of each gene. (F) Protein complexes enriched by COMPLEAT analysis related to autophagy, glycolysis, fatty acid biosynthesis, translation, mitochondria, and energy metabolism. For each complex pair, the one on the left represents the expression change in the fat body of 16 hrs starved larvae versus fed larvae while the one on the right represents the expression change in the fat body of 16 hrs starved larvae versus starved *CPSF5* mutants. Each node represents the protein member of each complex with red color for up-regulation or blue color for down-regulation. Edges represent protein-protein interactions. Complexes included at COMPLEAT are either from annotation or prediction (Hu et al., 2017) (G) Relative mRNA expression of genes involved in autophagy and metabolism. RNA extracted from larval fat bodies of fed wt, 16hr-starved wt, 16hr-starved $TSC2^{109}/TSC2^{109}$, 16hr-starved $CDK8^{K185}/Df(3L)AC1$, 16hr-starved DOA^{HD}/DOA^{DEM}, and 16hr-starved $CPSF5^{H11}/CPSF5^{H11}$, were subjected to qPCR analysis to detect gene expression. Compared with control under fed conditions, mRNAs involved in glucose catabolism (*l(1)G0334* and *Eno*), ribosome (*mRpL49, mRpL16,* and *mRpL17*) or energy metabolism (*ATPsynδ, ATPsynD, ND-MWFE,* and *ND-13A*) decreased in fat bodies from starved larvae, but not from *Tsc2, CDK8, DOA,* or *CPSF5* mutant larvae starved for 16 hrs. In contrast, mRNAs involved in autophagy (*Atg7* and *br*) and lipid catabolism (*Npc1a* and *Sdc*) increased in fat bodies from 16hr-starved larva, but not from *Tsc2, CDK8, DOA,* or *CPSF5* mutant larva starved for 16 hrs. *SRPK* mRNA did not show significant changes in any condition. One-Way ANOVA test was performed followed by Bonferroni's post hoc test. Measurements shown are mean ± SEM; *P<0.05, **P<0.01, ***P<0.001. (H) CDK8, DOA, and CPSF6 regulate lipid metabolism. Clonal expression of $CPSF6^{RNAi}$, DOA^{RNAi}, or $CDK8^{RNAi}$ in GFP-ATG8a labeled cells increased the size of lipid droplets stained by Nile red upon starvation. Scale bar, 20 μm. Quantification of the relative intensity of Nile red signals is shown (Student's T-test was performed to identify significant differences between Nile red signals in clones and signals in control cells outside of the clones; data represent as the mean± SEM of 3 fat-body samples imaged per genotype; *P<0.05, **P<0.01).

Figure S6. CDK8 and CLK2 interact with and phosphorylate CPSF6 to control its localization, RNA-binding ability, and autophagy in mammalian cells. Related to Figure 7.

(A) Human CPSF6 physically interacts with CDK8 and CLK2 under starvation conditions. HEK293T cells, transfected with GFP or GFP-tagged CPSF6, were incubated in nutrient rich medium (DMEM) or starvation medium (EBSS) for 2 hrs and subjected to immunoprecipitation (IP) with an anti-GFP nanobody. Immunoprecipitates and total cell lysates (TCL) were analyzed by immunoblotting (IB). (B) CDK8 and CLK2 are required for the starvation-induced phosphorylation of human CPSF6. Cells were cultured in DMEM or EBSS in the presence or absence of 50 μM Senexin-A (CDK8 inhibitor) or 50 μM TG003 (CLK2 inhibitor) for 2 hrs and then subjected to immunoprecipitation (IP). Immunoprecipitates and total cell lysates (TCL) were analyzed by immunoblotting (IB). (C) The CDK8 and CLK2-mediated phosphorylation of CPSF6 is essential for its association with RNAs. HEK293T cells transfected with GFP or GFP-CPSF6 were cultured in nutrient rich medium (DMEM) or starvation medium (EBSS) in the presence or absence of 50 μM Senexin-A (CDK8 inhibitor) or 50 μM TG003 (CLK2 inhibitor) for 2 hrs, and then subjected to RNA immunoprecipitations. Immunoprecipitated RNAs and RNAs of total cell lysates were analyzed by qRT-PCR with pairs of primers against *ULK1* and *LC3B.* Plotted fold change values (ratios of RNA IP/input normalized to GFP control) are the mean ± SEM of triplicates. One-Way ANOVA test was performed followed by Bonferroni's post hoc test. *P<0.05, **P<0.01. (D) Phosphorylation of CPSF6 by CDK8 or CLK2 is required for its nuclear targeting. MCF7 cells were cultured in DMEM or EBSS in the presence or absence of 50 μM Senexin-A (CDK8 inhibitor) or 50 μM TG003 (CLK2 inhibitor) for 2 hrs and then subjected to immunofluorescence analysis. CPSF6 was enriched in nuclei under fed or starvation conditions, whereas it redistributed to the cytoplasm when cells were treated with Senexin-A or TG003. Cells are stained with DAPI (blue). Scale bar, 10 mm. (E-F) CDK8, CLK2, and CPSF6 are required for

starvation-induced autophagosome formation. MCF7 cells were cultured in nutrient rich medium (DMEM) or starvation medium (EBSS) in the presence or absence of the lysosomal inhibitor Bafilomycin A1 (BafA1) for 2 hrs and subjected to immunofluorescence analysis. Compared to the nutrient rich conditions, the number of LC3 punctae were increased by starvation. Treatment of 50 μM Senexin-A (CDK8 inhibitor) or 50 μM TG003 (CLK2 inhibitor) (E), or infection with lentivirus expressing *CPSF6* shRNA (F) inhibited EBSS-induced LC3 punctae formation. shLuc is used as control. LC3 was stained with LC3B antibody (green) and nuclei were stained with DAPI (blue). Scale bar, 10 μm.

Figure S7. Model of autophagy and metabolism regulation by TORC1/CDK8/DOA/CPA. Related to Figure 7.

(A-B) TORC1 promotes the ubiquitination and degradation of CDK8 and DOA/CLK2 (A). In response to nutrient deprivation, where TORC1 activity is reduced, CDK8 and DOA/CLK2 protein levels are up-regulated, which in turn leads to CPSF6 phosphorylation that enhances its RNA binding ability and promotes APA and AS of transcripts related to autophagy and metabolism. APA-induced *Atg1-RA* transcripts possess long 3'UTRs that stabilize them. In addition, AS-induced *Atg1-RA* transcripts encode a kinase that escapes the inhibition by PKA, thus leading to induction of autophagy. These alternate RNA processing events also suppress lipid, protein, and energy metabolism (B). (C) Moreover, as TORC1 is hyperactivated, CPSF6 phosphorylation is blocked and CPSF6 translocates to the cytoplasm, further inhibiting autophagy and enhancing lipid, protein, and energy metabolism.

Figure S1

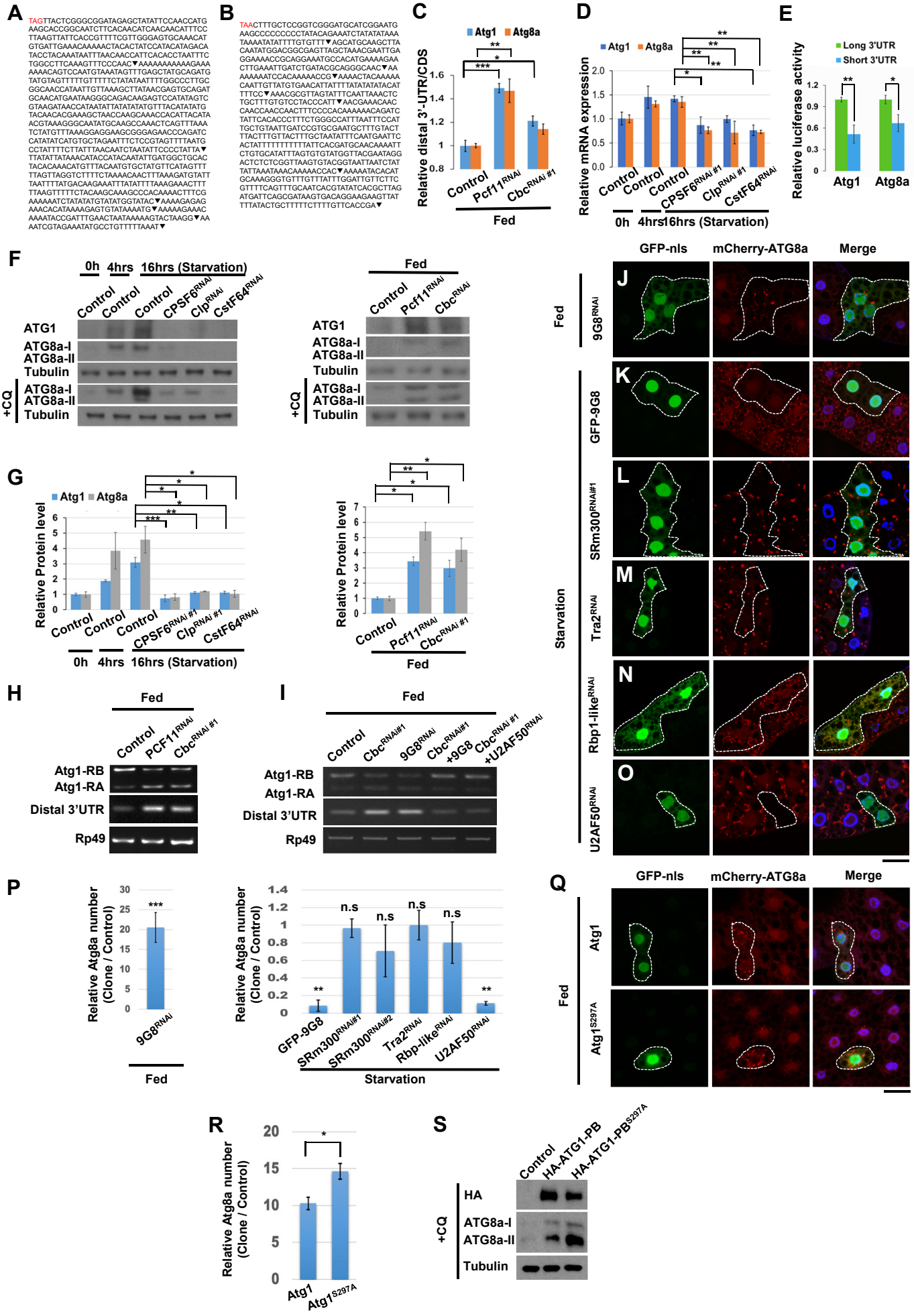
A
B
C
Atg1
Atg8a
Relative distal 3'-UTR/CDS
Control
Pcf11RNAi
CbcRNAi #1
Fed
D
Relative mRNA expression
Control
CPSF6RNAi #1
ClpRNAi #1
CstF64RNAi
0h
4hrs
16hrs (Starvation)
E
Long 3'UTR
Short 3'UTR
Relative luciferase activity
F
ATG1
ATG8a-I
ATG8a-II
Tubulin
+CQ
G
Relative Protein level
H
Atg1-RB
Atg1-RA
Distal 3'UTR
Rp49
PCF11RNAi
I
CbcRNAi#1
9G8RNAi
CbcRNAi#1 +9G8
CbcRNAi #1 +U2AF50RNAi
J
GFP-nls
mCherry-ATG8a
Merge
9G8RNAi
K
GFP-9G8
L
SRm300RNAi#1
M
Tra2RNAi
N
Rbp1-likeRNAi
O
U2AF50RNAi
Starvation
P
Relative Atg8a number (Clone / Control)
n.s
GFP-9G8
SRm300RNAi#1
SRm300RNAi#2
Tra2RNAi
Rbp-likeRNAi
U2AF50RNAi
Q
Atg1
Atg1S297A
R
S
HA-ATG1-PB
HA-ATG1-PBS297A
HA

Figure S2

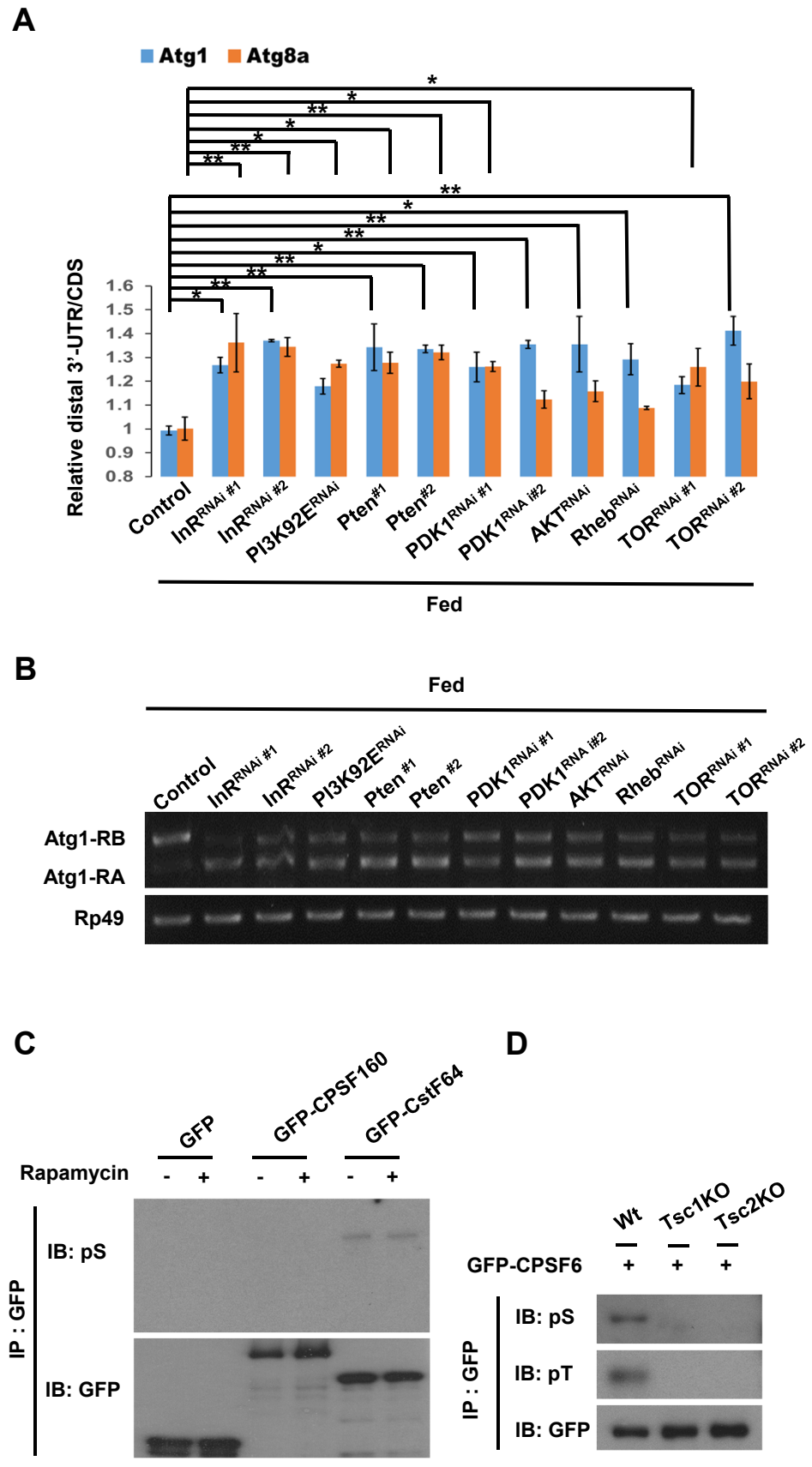
A
Atg1
Atg8a
Relative distal 3'-UTR/CDS
1.6
1.5
1.4
1.3
1.2
1.1
1
0.9
0.8
Control
InR RNAi #1
InR RNAi #2
PI3K92E RNAi
Pten #1
Pten #2
PDK1 RNAi #1
PDK1 RNA i#2
AKT RNAi
Rheb RNAi
TOR RNAi #1
TOR RNAi #2
Fed
B
Fed
Control
InR RNAi #1
InR RNAi #2
PI3K92E RNAi
Pten #1
Pten #2
PDK1 RNAi #1
PDK1 RNA i#2
AKT RNAi
Rheb RNAi
TOR RNAi #1
TOR RNAi #2
Atg1-RB
Atg1-RA
Rp49
C
GFP
GFP-CPSF160
GFP-CstF64
Rapamycin
- + - + - +
IP : GFP
IB: pS
IB: GFP
D
Wt
Tsc1KO
Tsc2KO
GFP-CPSF6
+ + +
IP : GFP
IB: pS
IB: pT
IB: GFP

Figure S3

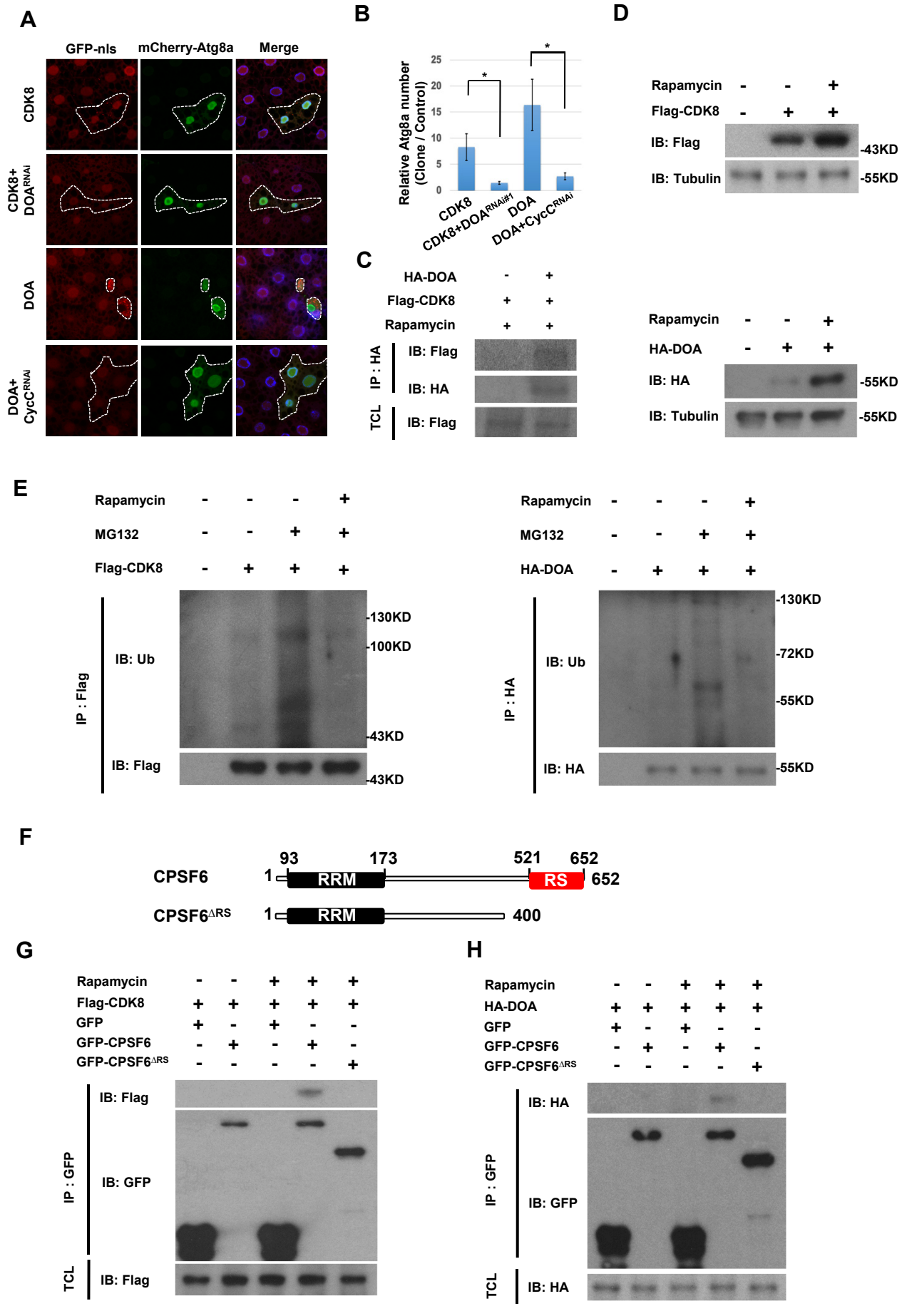
A
GFP-nls
mCherry-Atg8a
Merge
CDK8
CDK8+ DOA^RNAi
DOA
DOA+ CycC^RNAi
B
Relative Atg8a number (Clone / Control)
25
20
15
10
5
0
*
*
CDK8
CDK8+DOA^RNAi#1
DOA
DOA+CycC^RNAi
C
HA-DOA - +
Flag-CDK8 + +
Rapamycin + +
IP : HA
IB: Flag
IB: HA
TCL
IB: Flag
D
Rapamycin - - +
Flag-CDK8 - + +
IB: Flag
-43KD
IB: Tubulin
-55KD
Rapamycin - - +
HA-DOA - + +
IB: HA
-55KD
IB: Tubulin
-55KD
E
Rapamycin - - - +
MG132 - - + +
Flag-CDK8 - + + +
IP : Flag
IB: Ub
-130KD
-100KD
-43KD
IB: Flag
-43KD
Rapamycin - - - +
MG132 - - + +
HA-DOA - + + +
IP : HA
IB: Ub
-130KD
-72KD
-55KD
IB: HA
-55KD
F
CPSF6
1
93
173
521
652
RRM
RS
652
CPSF6^ΔRS
1
RRM
400
G
Rapamycin - - + + +
Flag-CDK8 + + + + +
GFP + - + - -
GFP-CPSF6 - + - + -
GFP-CPSF6^ΔRS - - - - +
IP : GFP
IB: Flag
IB: GFP
TCL
IB: Flag
H
Rapamycin - - + + +
HA-DOA + + + + +
GFP + - + - -
GFP-CPSF6 - + - + -
GFP-CPSF6^ΔRS - - - - +
IP : GFP
IB: HA
IB: GFP
TCL
IB: HA

Figure S4

A

Drosophila CPSF6 (401aa - 652aa)

MNMTPQHGPP PQFAQHGPRG PWPPPQGKPP GPFPDPQQMG PQLTEVEFEE
VMSRNRTVSS SAIARAVSDA AAGEYSSAIE TLVTAISLIK QSKVAHDERC
KILISSLQDT LHGIEAKSYN RRERSRSRER SHRSRQRRER STSRYRERSR
ERERDRDRER ERDGGSYRER SRSRERERQA PDHYRDDSRS VRPRKSPEPV
VAEAAEAPSS KRYYEDRERY RSSDRERRDR DRDRDRERER DRDRREEHRS
RH

S588 S596

: CDK8 consensus phosphorylation sites
: DOA consensus phosphorylation sites
: CDK8 phosphorylation site identified in in-vitro kinase assay
: DOA phosphorylation site identified in in-vitro kinase assay

B

	Peptide sequence	DMSO		Rapamycin	
		Total-ion-current	Occupancy	Total-ion-current	Occupancy
pS588 S588	RDDpSRSVRPRKSPEPVVAEAAEAPSSKRY RDDSRSVRPRKSPEPVVAEAAEAPSSKRY	0 7473527.7	0%	210073 5009806.6	4.02%
pS596 S596	RDDSRSVRPRKpSPEPVVAEAAEAPSSKRY RDDSRSVRPRKSPEPVVAEAAEAPSSKRY	3422309.5 4051218.2	45.79%	3176605 2043274.6	60.86%

C

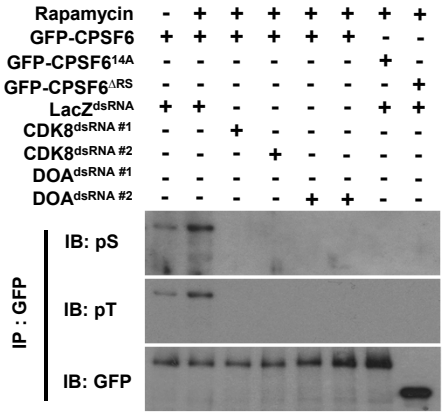

D

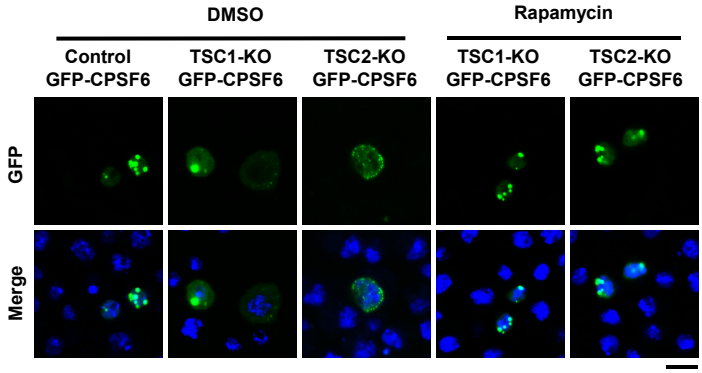

E

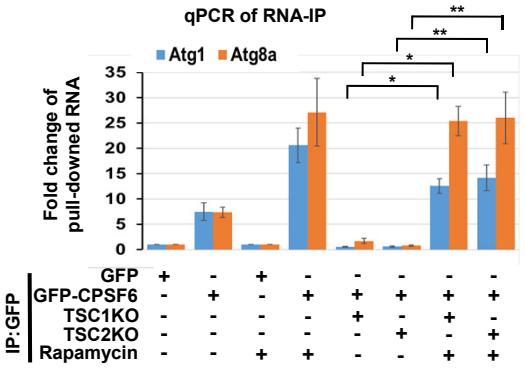

F

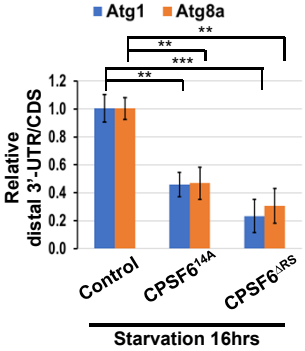

G

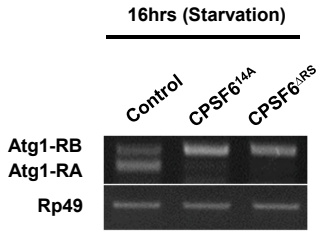

H

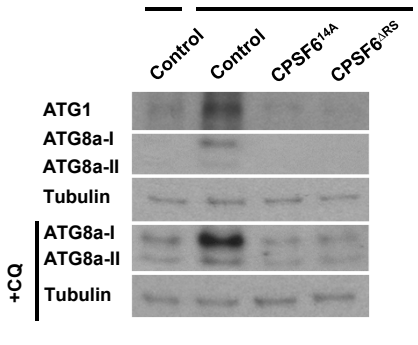

I

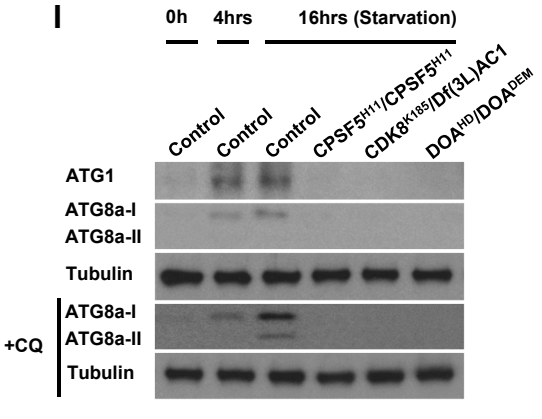

Figure S5

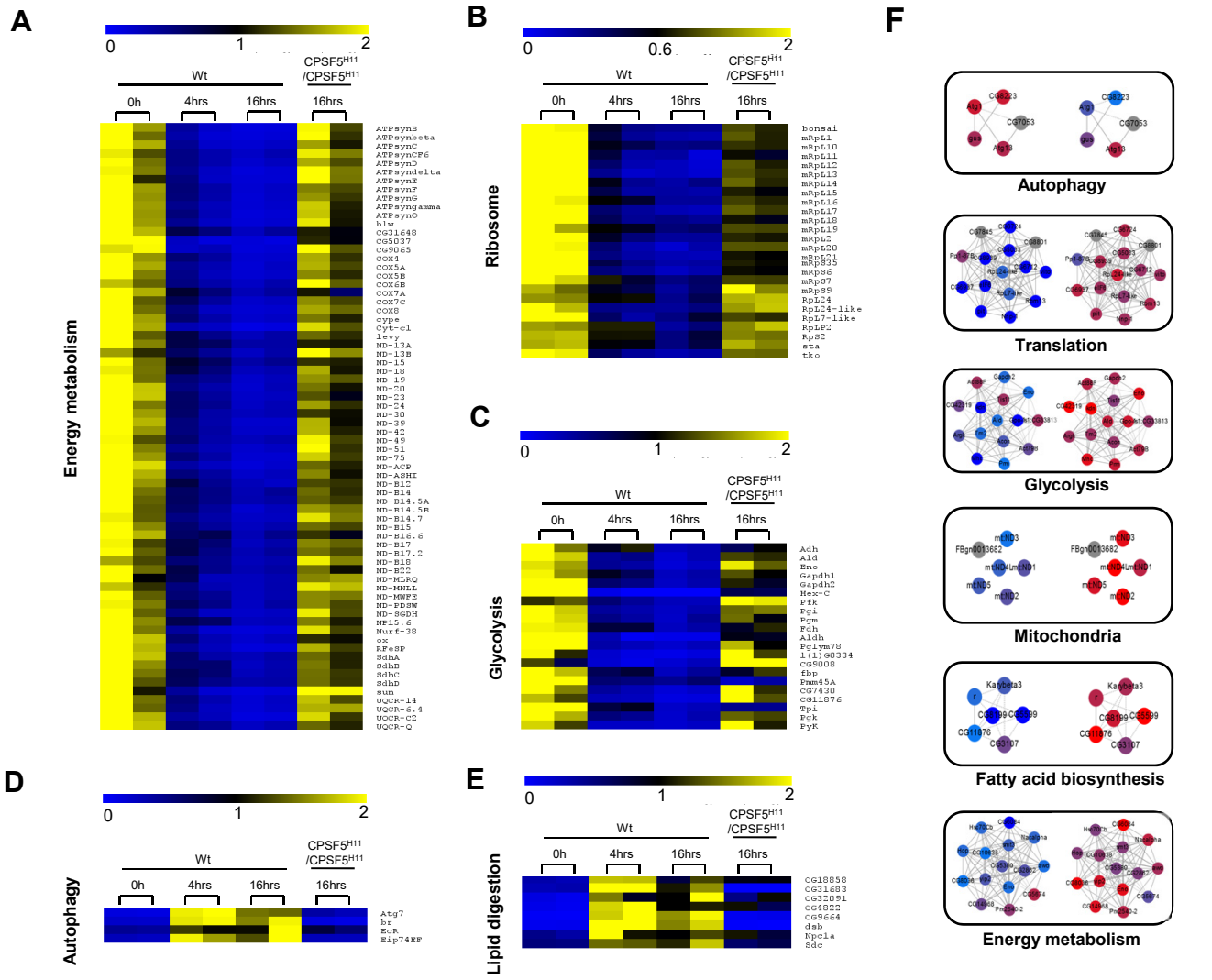
A
B
C
D
E
F
Wt
CPSF5H11 /CPSF5H11
0h
4hrs
16hrs
Energy metabolism
Ribosome
Glycolysis
Autophagy
Lipid digestion
Autophagy
Translation
Glycolysis
Mitochondria
Fatty acid biosynthesis
Energy metabolism

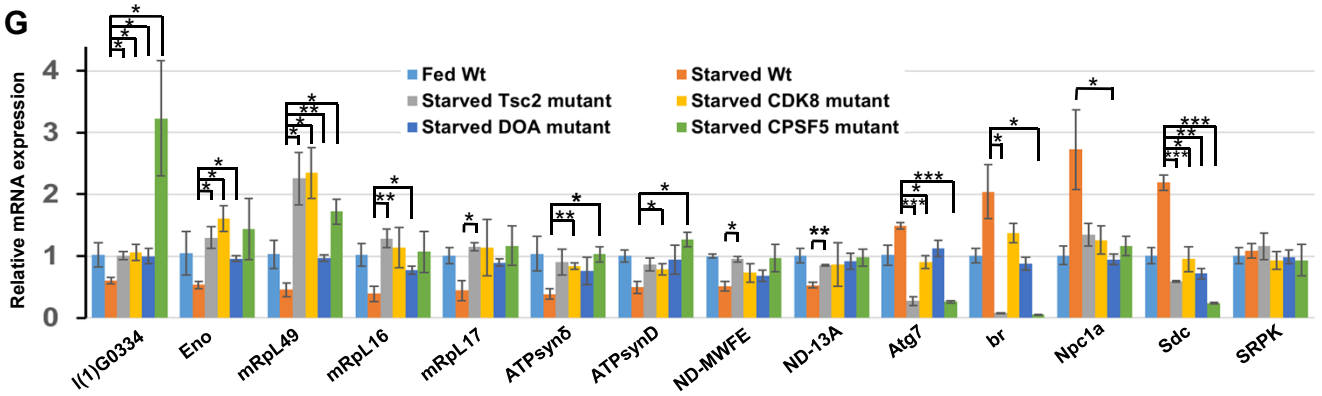
G
Relative mRNA expression
Fed Wt
Starved Wt
Starved Tsc2 mutant
Starved CDK8 mutant
Starved DOA mutant
Starved CPSF5 mutant
l(1)G0334
Eno
mRpL49
mRpL16
mRpL17
ATPsyn5
ATPsynD
ND-MWFE
ND-13A
Atg7
br
Npc1a
Sdc
SRPK

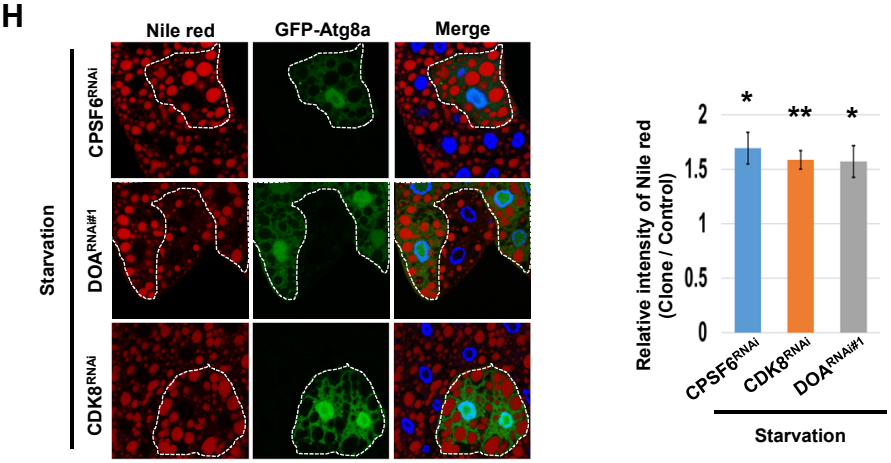
H
Nile red
GFP-Atg8a
Merge
Starvation
CPSF6RNAi
DOARNAi#1
CDK8RNAi
Relative intensity of Nile red (Clone / Control)
Starvation

Figure S6

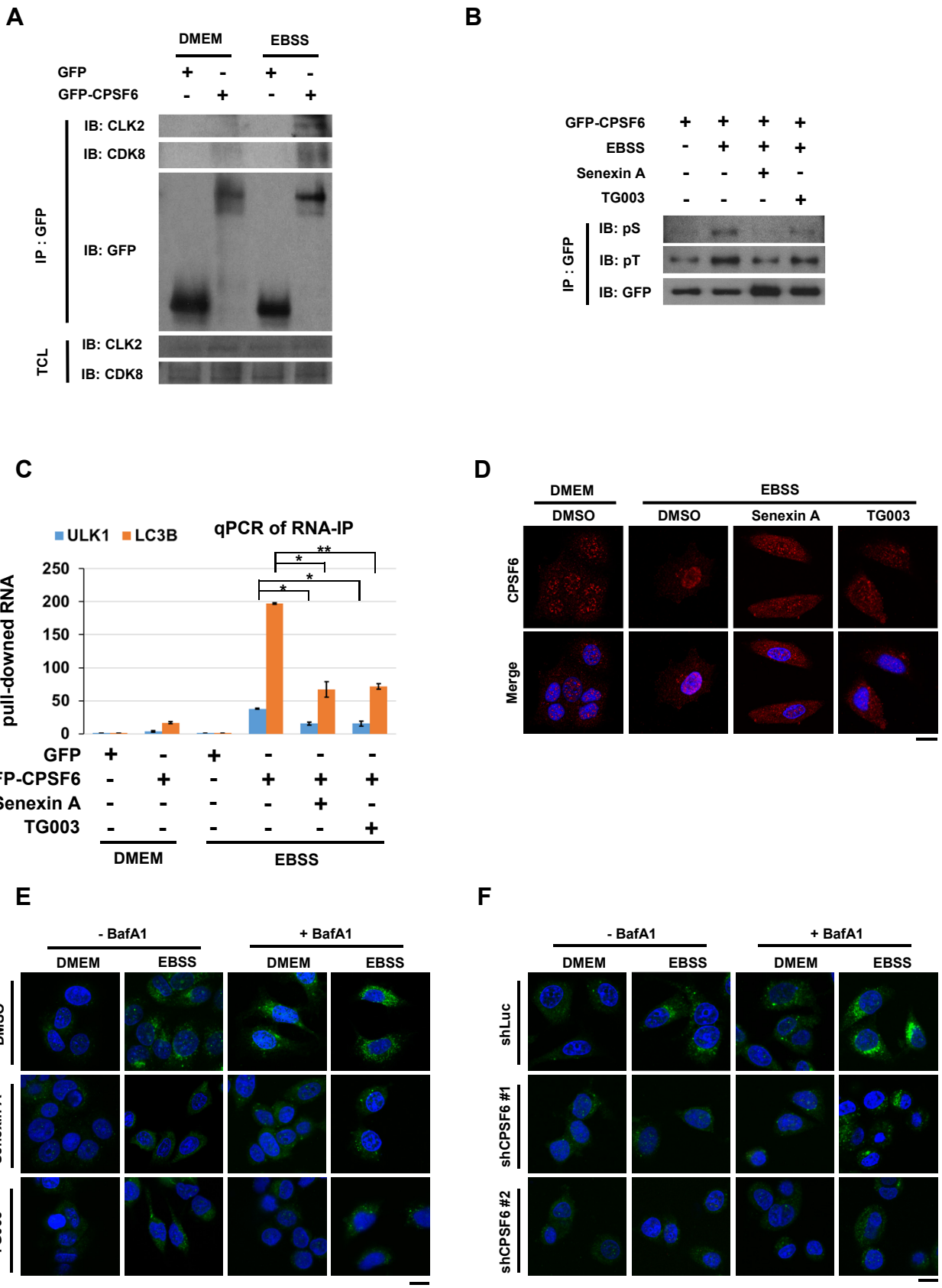
A
DMEM
EBSS
GFP
GFP-CPSF6
IB: CLK2
IB: CDK8
IB: GFP
IP : GFP
TCL
IB: CLK2
IB: CDK8
B
GFP-CPSF6
EBSS
Senexin A
TG003
IB: pS
IB: pT
IB: GFP
IP : GFP
C
ULK1
LC3B
qPCR of RNA-IP
Fold change of pull-downed RNA
250
200
150
100
50
0
GFP
GFP-CPSF6
Senexin A
TG003
IP:GFP
DMEM
EBSS
D
DMEM
EBSS
DMSO
DMSO
Senexin A
TG003
CPSF6
Merge
E
- BafA1
+ BafA1
DMEM
EBSS
DMEM
EBSS
DMSO
Senexin A
TG003
F
- BafA1
+ BafA1
DMEM
EBSS
DMEM
EBSS
shLuc
shCPSF6 #1
shCPSF6 #2

Figure S7

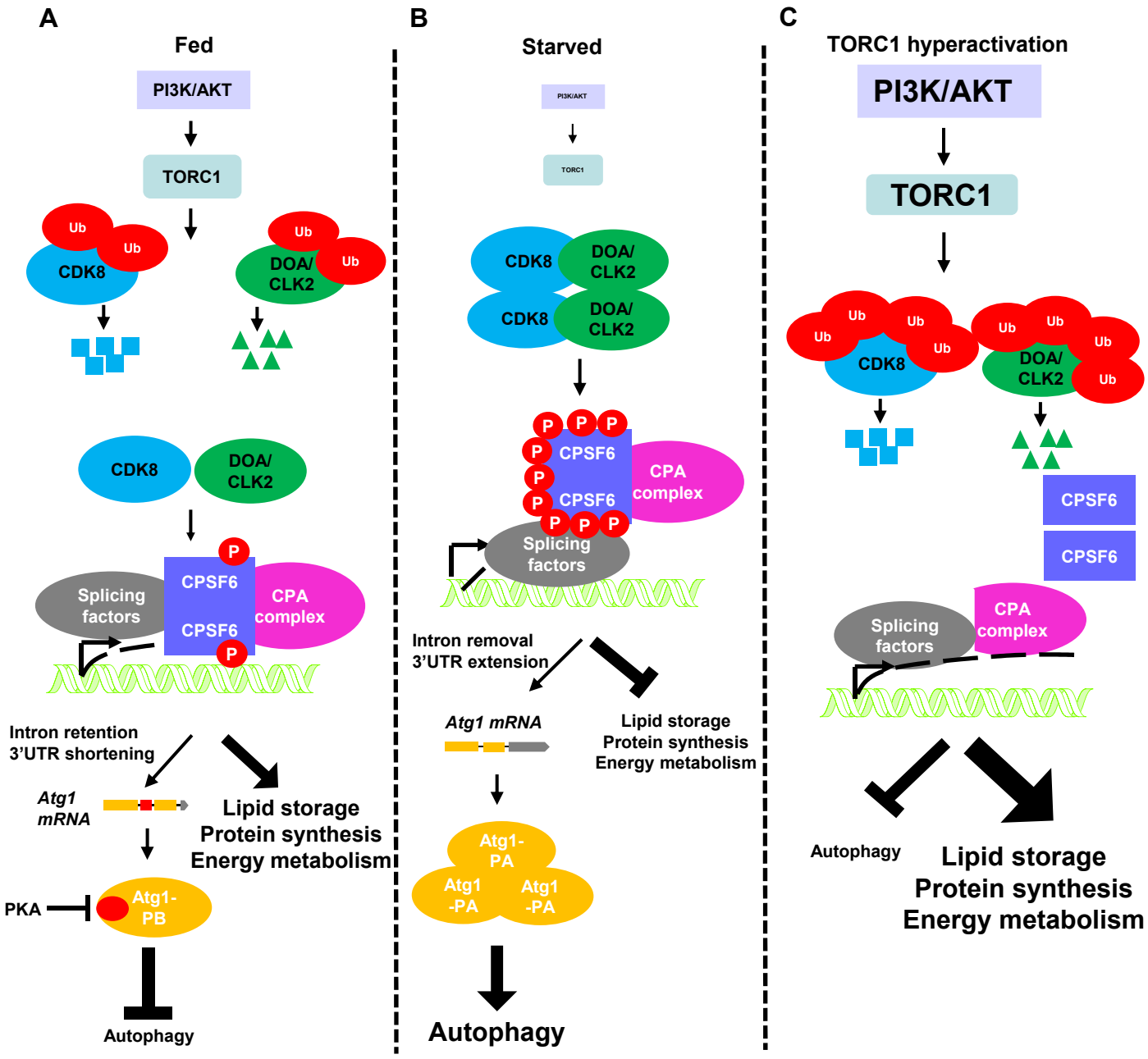
A
Fed
PI3K/AKT
TORC1
Ub
CDK8
DOA/
CLK2
CPSF6
CPA
complex
Splicing
factors
P
Intron retention
3'UTR shortening
Atg1
mRNA
Lipid storage
Protein synthesis
Energy metabolism
PKA
Atg1-
PB
Autophagy
B
Starved
Intron removal
3'UTR extension
Atg1 mRNA
Atg1-
PA
Atg1
-PA
Lipid storage
Protein synthesis
Energy metabolism
Autophagy
C
TORC1 hyperactivation
PI3K/AKT
TORC1
CPSF6
Autophagy
Lipid storage
Protein synthesis
Energy metabolism